MAGNETIC BEARING REACTION WHEEL

FINAL REPORT

JPL CONTRACT NO. 954143

This work was performed for the Jet Propulsion Laboratory, California Institute of Technology sponsored by the National Aeronautics and Space Administration under Contract NAS7-100.

PREPARED BY

Ajit Sabnis
A. Sabnis

F. Schmitt
F. Schmitt

L. Smith
L. Smith

APPROVED BY

J. R. Dohogne
J. R. Dohogne

SPERRY
FLIGHT SYSTEMS

PHOENIX, ARIZONA

COPY NO. _____

PRINTED IN U.S.A.

FEBRUARY 1976

PUB. NO. 71-0853-00-00

TECHNICAL CONTENT STATEMENT

This report contains information prepared by Sperry Flight Systems under JPL subcontract. Its content is not necessarily endorsed by the Jet Propulsion Laboratory, California Institute of Technology, or the National Aeronautics and Space Administration.

ABSTRACT

The results of a program for the development, fabrication and functional test of an engineering model magnetically suspended reaction wheel are described in this report. The reaction wheel develops an angular momentum of ±.5 foot-pound-second and is intended for eventual application in the attitude control of long-life interplanetary and orbiting spacecraft. A description of the wheel design and its major performance characteristics is presented. Recommendations for flight prototype development are made.

SUMMARY

This report describes the results of a program for the development of an engineering model Magnetic Bearing Reaction Wheel (MBRW). The intended application for the MBRW is in the attitude control of long life interplanetary and orbiting spacecraft. The primary advantages sought through the use of magnetic suspension are long life, high reliability, low induced vibration and precise control characteristics. The elimination of surface contact enables wear-free, vacuum-compatible, unlubricated operation. In addition, it was desired to minimize wheel weight and particularly power to meet typical outer-planet spacecraft functional requirements.

A photograph of the MBRW and its associated electronics assembly is shown in Figure i-1 and the outline drawing with overall dimensions is shown in Figure i-2. The design concept evolved in a prior study* was used as the baseline for the detailed design of the MBRW: the major differences were the addition of a high-resolution tachometer and the provision of complete redundancy in the electronics. Two passive-radial, active-axial magnetic bearings were used for the suspension system. This arrangement also permits the achievement of transverse angular stability by passive means, and requires active servo control in only the axial direction. The axial control force is generated by modulating the permanent magnet fields; a positive integral feedback in the control loop minimizes power consumption and sensitivity to electronic component drift.

A large diameter ac induction motor with segmented stators enables efficient use of the motor rotor mass to provide a significant portion of the rotational inertia, while permitting full functional redundancy. The MBRW rotor is umbrella-shaped, and has integrally machined teeth for use in the tachometer system. A ball-bearing touchdown system provides rotational support when the axial control system is inoperative, and also prevents physical contact at the magnetic bearing gaps, the motor gap and the tachometer probe gaps.

Functional tests were conducted on the MBRW, including suspension characteristics, torque characteristics and power measurements. Major MBRW parameters are listed in Table i-1. Functional testing of the MBRW was successful and the parameter comparison confirms the feasibility of the approach for a flight design.

---

*Final Report: "Design Study for a Magnetically Supported Reaction Wheel," JPL Contract No. 953884, Sperry Flight Systems Pub. No. 71-0489-00-00, July 1974.

Areas of departure from the predicted design values and the requisite design modifications are discussed in the report. The section on conclusions and recommendations identifies areas which would probably require effort in a subsequent program for development of flight hardware.

TABLE i-1

MAJOR MBRW PARAMETERS

Parameter	Design Requirement	Attained Value
Angular Momentum	±.5 ft-lb-sec	±.5 ft-lb-sec (at ±700 rpm)
Weight*	8.0 pounds	8.9 pounds**
Output torque (minimum)	.02 ft-lb	.02 ft-lb
Power		
• Motor		
(a) at .007 ft-lb torque	4.2 watts	3.62 watts
(b) at .02 ft-lb torque	12 watts	9.56 watts
• Bearing (steady-state)	.5 watt	.67 watt
Calculated Reliability (10 years)	.98	.995
Tachometer	360 pulses/rev	520 pulses/rev
Size	9 inch diameter (maximum)	8.9 inch diameter 6 inches axial length

*Including estimated weight of flight-type redundant suspension electronics but excluding the weight of the tachometer electronics, as defined in the Design Requirements.

**The 700 rpm design point was chosen as a lower-power option by JPL because of the sensitivity to power in anticipated outer-planet missions. Choice of a 1000 rpm maximum speed would result in a MBRW weight of 8.2 pounds and still meet power requirements. Use of magnesium instead of aluminum for the housing would lower the MBRW weight further, to 7.5 pounds.

716 5 30

Figure i-1
MBRW and Associated Electronics Assembly

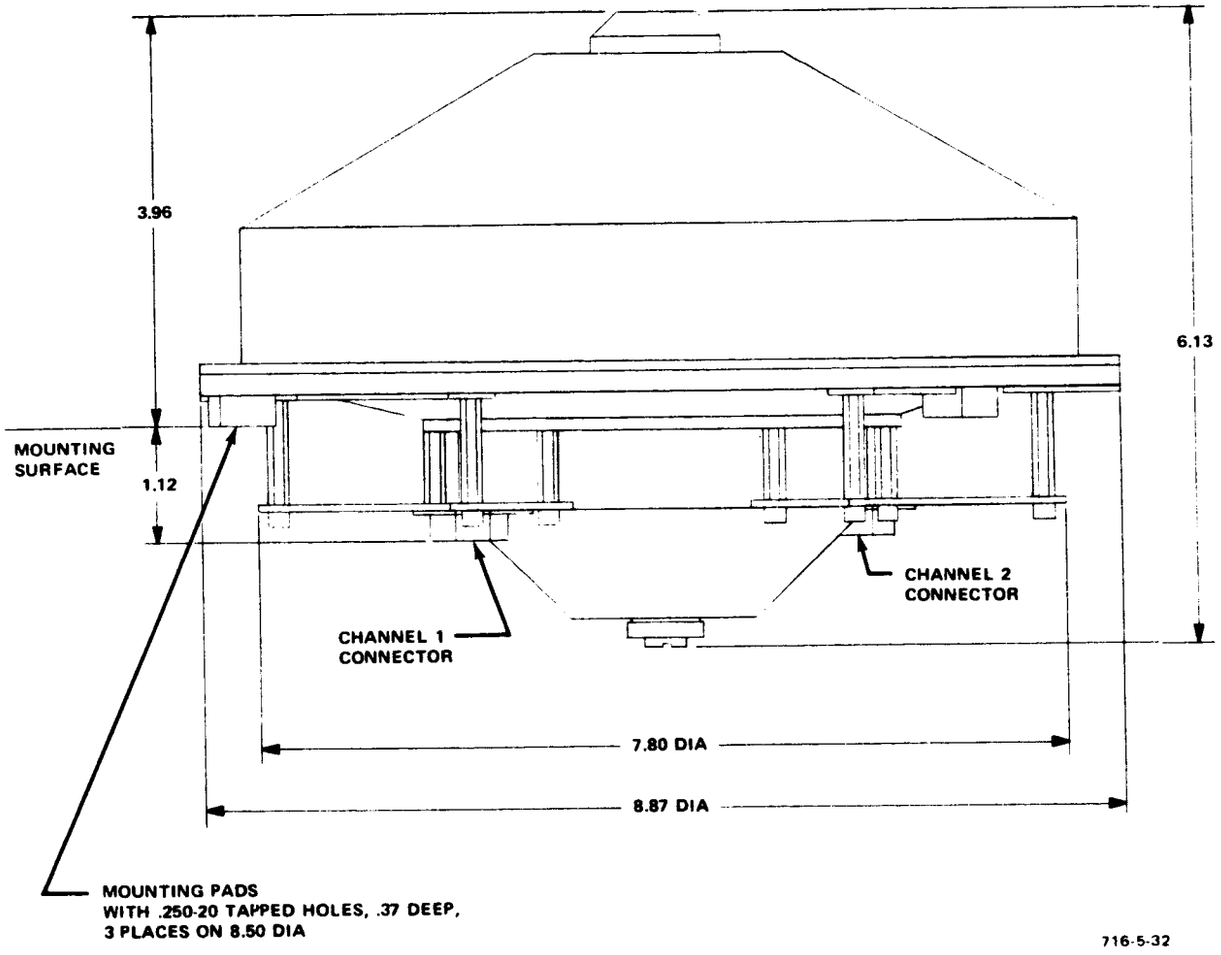

Figure i-2
MBRW Outline

TABLE OF CONTENTS

TABLE OF CONTENTS (cont)

LIST OF ILLUSTRATIONS

LIST OF ILLUSTRATIONS (cont)

SECTION 1.0

INTRODUCTION

SECTION 1.0

INTRODUCTION

1.1 BACKGROUND

The use of Reaction Wheel Assemblies (RWAs) is a demonstrated technique for precise attitude control of spacecraft. In a typical system, three orthogonally mounted RWAs are employed, each developing bidirectional control torques about a spacecraft axis in response to attitude sensor signals.

For anticipated future outer-planet spacecraft applications, RWA operating life is of prime interest. Ball bearing supported wheels have achieved lifetimes in the neighborhood of 5 years, but their continuous use for 10 year missions is open to question. This is primarily because of the necessity of assuring the presence of a lubricant in the ball contact area over the required time, and of providing a load-carrying film (boundary lubrication) in the region of zero spin speed.

The obvious solution to the problem is to avoid metal-to-metal contact in the suspension elements, and to eliminate the need for lubrication. Magnetic suspension constitutes such a contactless support system and forms the basis of the RWA development described in this report.

The feasibility of using magnetic bearings in a reaction wheel for interplanetary and orbiting spacecraft was examined in a prior design study (JPL Contract No. 953884). It was concluded that a Magnetic Bearing Reaction Wheel (MBRW) would be competitive with ball bearing designs in terms of size, weight, power and cost.

Following the design study, a program for the detailed design, fabrication and functional testing of an engineering model MBRW was initiated (JPL Contract No. 954143) in order to confirm the conclusions of the study. The primary differences from the requirements of the study were the inclusion of complete redundancy in the system and the incorporation of a high-resolution tachometer. The tachometer is intended to be used for precise control of MBRW rotational speed in a speed control loop. This report describes the results of the development effort and is submitted in partial fulfillment of JPL Contract No. 954143.

1.2 TECHNICAL APPROACH

The fundamental objective of the program was considered to be the development and functional evaluation of an engineering model Magnetic Bearing Reaction Wheel (MBRW). The use of magnetic suspension enables the reaction wheel to possess the characteristics of long life and high reliability, low power consumption and precise control characteristics.

The design of the engineering model MBRW was approached as being a flight design; however, existing hardware and techniques were used in the interest of economics and schedule, and as a high-confidence approach to achieving the program goal.

Thus, the one-loop bearing system concept previously developed at Sperry was used for the magnetic suspension; similarly, an existing 7 inch diameter segmented ac induction motor was used in the design. The one-loop bearing design was extrapolated from the design tested in the Sperry one-loop model.

The design considered as a baseline was that evolved in the design study, JPL Contract No. 953884, with the addition of a high-resolution tachometer. Results from on-going magnetic suspension development work at Sperry were also incorporated into the RWA design.

Design point selection was based on weight optimization, subject to the motor power constraint. The design incorporated complete redundancy of all systems (suspension, tachometer and motor) in order to eliminate all single-point failures.

The remainder of this report is organized as follows: Section 2.0 presents a detailed description of the MBRW design, Section 3.0 contains the results of MBRW testing, and the conclusions and recommendations are outlined in Section 4.0.

The instructions for installation and operation of the MBRW are contained in a separate publication, "Operation Manual: Magnetic Bearing Reaction Wheel," Sperry Flight Systems Pub. No. 71-0847-00-00.

SECTION 2.0

DESIGN OF THE ENGINEERING MODEL MAGNETIC BEARING REACTION WHEEL

SECTION 2.0

DESIGN OF THE ENGINEERING MODEL MAGNETIC BEARING REACTION WHEEL

2.1 SYSTEM CONFIGURATION

A block diagram of the MBRW system is shown in Figure 2-1. The system consists of two separate subassemblies:

- Magnetic Bearing Reaction Wheel (MBRW)
- MBRW Electronics Assembly

The MBRW consists of the rotor, segmented ac induction motors, magnetic bearings, touchdown bearings, axial position sensor probes and the tachometer, all in a sealed housing. The MBRW is, however, designed to be vented to the space vacuum environment in actual spacecraft operation. The required electronics for the suspension system, the tachometer system and for monitoring are mounted in the Electronics Assembly, except for the position sensor drive electronics, which are mounted on two boards on the underside of the MBRW. The Electronics Assembly is in breadboard form and is designed to be rack-mounted.

Two separate, identical electronics channels are provided for both the suspension and the tachometer. Redundancy of the spin motor function is possible because a segmented motor construction is used. Thus, redundancy requires the use of separate motor stators but not separate rotors since the rotor is a passive electromagnetic element. The motor leads are brought out to the Electronics Assembly. The present design thus permits open-loop sine-wave or square-wave motor drive, and allows for future incorporation of a spin motor control system.

The monitoring electronics is non-redundant and provides indications of suspension and wheel speed. An overspeed light turns on at 750 rpm, nominal maximum speed being 700 rpm. Two separate cables provide identical position, tachometer, motor and control coil interconnections between the MBRW and the Electronics Assembly. Separate channel select switches enable choice of either suspension, tachometer or motor channel; a master switch disconnects all power from the entire system. The MBRW system operates off +28 volts, ±15 volts, and +5 volts laboratory power supplies; the motor is driven by a 0 to 28 volt, 2 phase, 280 Hz supply.

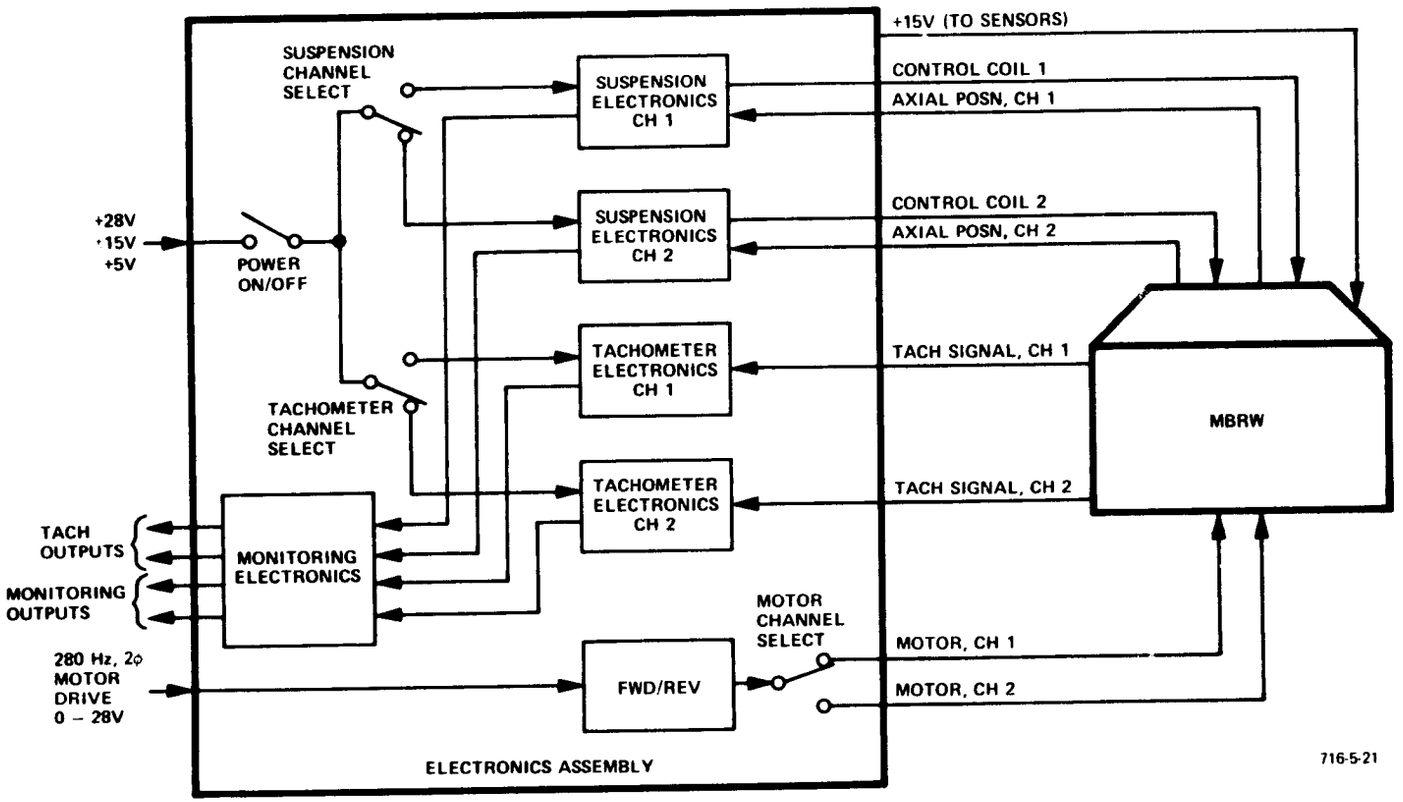

Figure 2-1
MBRW System Configuration

2.2 DESIGN REQUIREMENTS AND OBJECTIVES

The important design requirements and goals for the MBRW are listed in Table 2-1. The table also shows the values attained in the actual design, and the method by which these values were verified. Discussion of the attained values in relation to the requirements and goals is contained in the appropriate sections describing the design and/or the test results. References to these sections are given in the table.

2.3 MBRW DESIGN AND CONSTRUCTION

Minimization of the weight and size of the MBRW was a major consideration for the design. Other constraints which also had direct effects were the requirement for no single point failures, reduction of peak torquing power, and the use of existing spin motor and magnetic bearing designs. The final design layout is shown in Figure 2-2.

The MBRW design layout can be divided into two major assemblies - the rotor assembly and the housing assembly.

a. Rotor Assembly

An "umbrella" rotor configuration was selected because of the need for a high axial stiffness between magnetic bearing rotors and stators, and the compactness gained by placing the magnetic bearing rotors outboard of the stators. The rotor assembly is shown in Figure 2-3. The achievement of positive angular stiffness dictates a minimum axial separation between the two radial-passive bearings. Since the stators extend further from the gaps than the rotors, overall axial length is minimized by placing the stators inboard. The umbrella design also provides better control of rotor, bearing and shaft geometry and permits easy disassembly of the rotor from the housing.

The spin motor stator segments are placed midway between bearings to prevent possible angular motions of the rotor due to any radial unbalance force of the motor. This placement of the motor and rotor rim allows use of a conical web which provides a high hub-to-rim stiffness. Access holes through the rotor web at four places enable tachometer probe adjustments to be made without removing the rotor assembly.

TABLE 2-1

DESIGN REQUIREMENTS, GOALS AND ATTAINED VALUES

Characteristic	Design Requirement	Design Goal	Value Attained	Verified By	Reference
Angular Momentum	±.5 ft-lb-sec		±.5 ft-lb-sec	Measurement	
Weight	8.0 pounds		8.9 pounds	Measurement	Section 2.4
Size (maximum dimension)		9 inches	8.9 inches	Measurement	
Tachometer Output	360 pulses/rev, Direction of rotation signal	1200 pulses/rev	520 pulses/rev, Direction of rotation signal provided	Measurement	Section 2.8 and 3.4
Output Torque and Motor Power	(a) .007 ft-lb, 4.2 watts (b) .02 ft-lb, 12 watts		(a) .007 ft-lb, 3.62 watts (b) .02 ft-lb, 9.6 watts	Measurement	Section 3.3
Bearing Power					
Liftoff	15 watts maximum (< 5 msec)		39.2 watts maximum	Measurement	Section 3.2
Operating	.5 watt	.25 watt	.67 watt		
Capacity in 1g	Operation in any attitude		Operation with spin axis vertical and within 20° of vertical	Observation	Section 3.1
Axial Damping Coefficient	.6		.7	Measurement	Section 3.2
Axial Step Response	6 msec		4 msec		
Resonant Frequencies	Above maximum speed and ≥ 20 Hz		9 Hz (zero speed angular) 29 Hz (radial)	Measurement	Section 3.1
Reliability (10 years)	.98		.995	Analysis	Section 2.10
Balance					
Static	.05 oz-in	.005 oz-in	.0035 oz-in	Measurement	Section 3.1 and Appendix A
Dynamic	.5 oz-in^2	.05 oz-in^2	.019 oz-in^2		
External Field at 1 meter*					
DC		10 nT		Not measured	
Variable		4 nT			
Environment*					
Shock and Vibration (Launch and Operating)	Per JPL Specification MJS77-3-240		MBRW designed for launch survivability and operation without degradation	Analysis	
Temperature	-20° to +75°C		MBRW designed for operation over temperature and pressure range	Analysis	
Pressure	+760 torr to 10^{-14} torr				

*Measurement of the external magnetic field characteristics and environmental performance tests were outside the scope of the program.

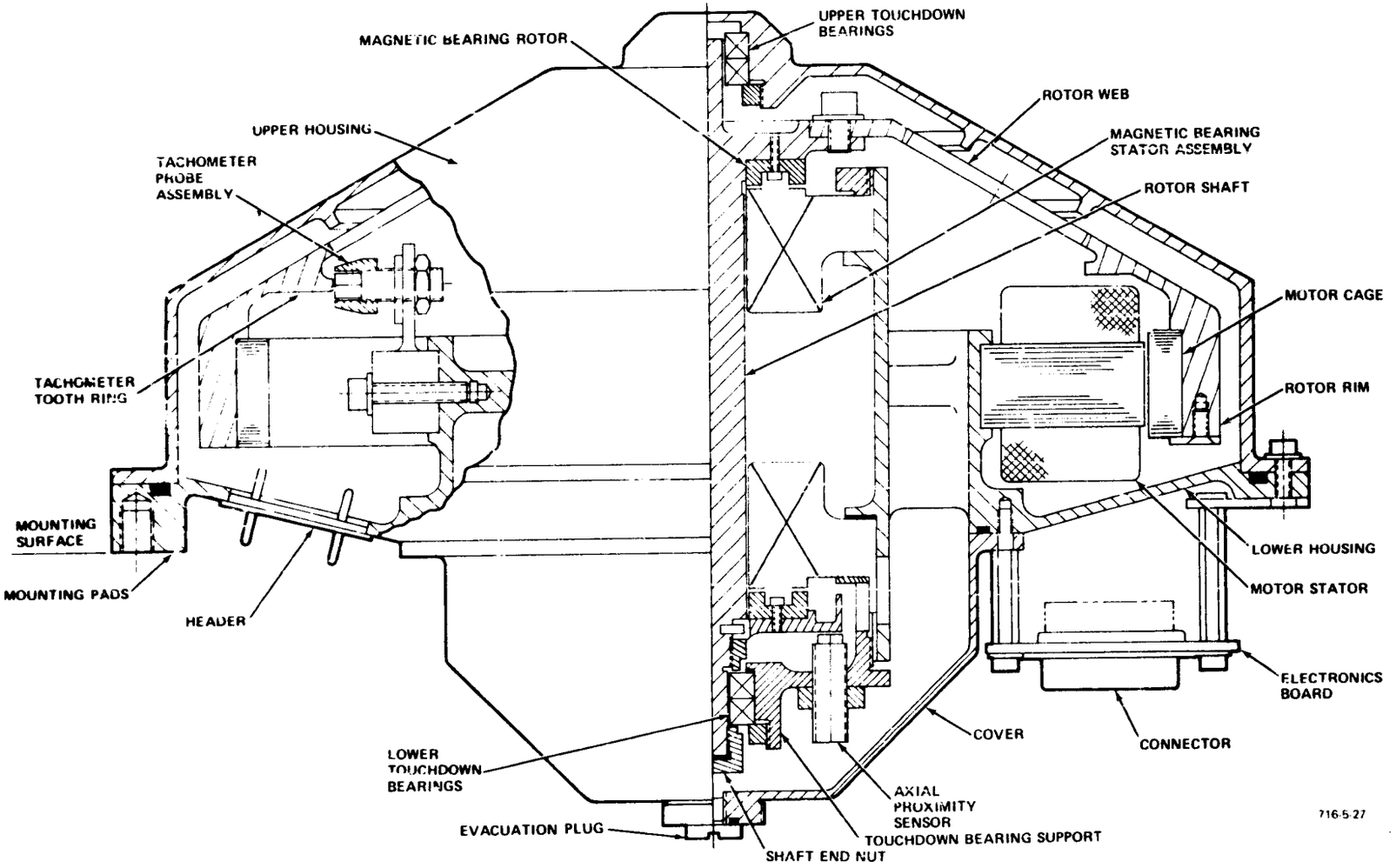

Figure 2-2
MBRW Design Layout

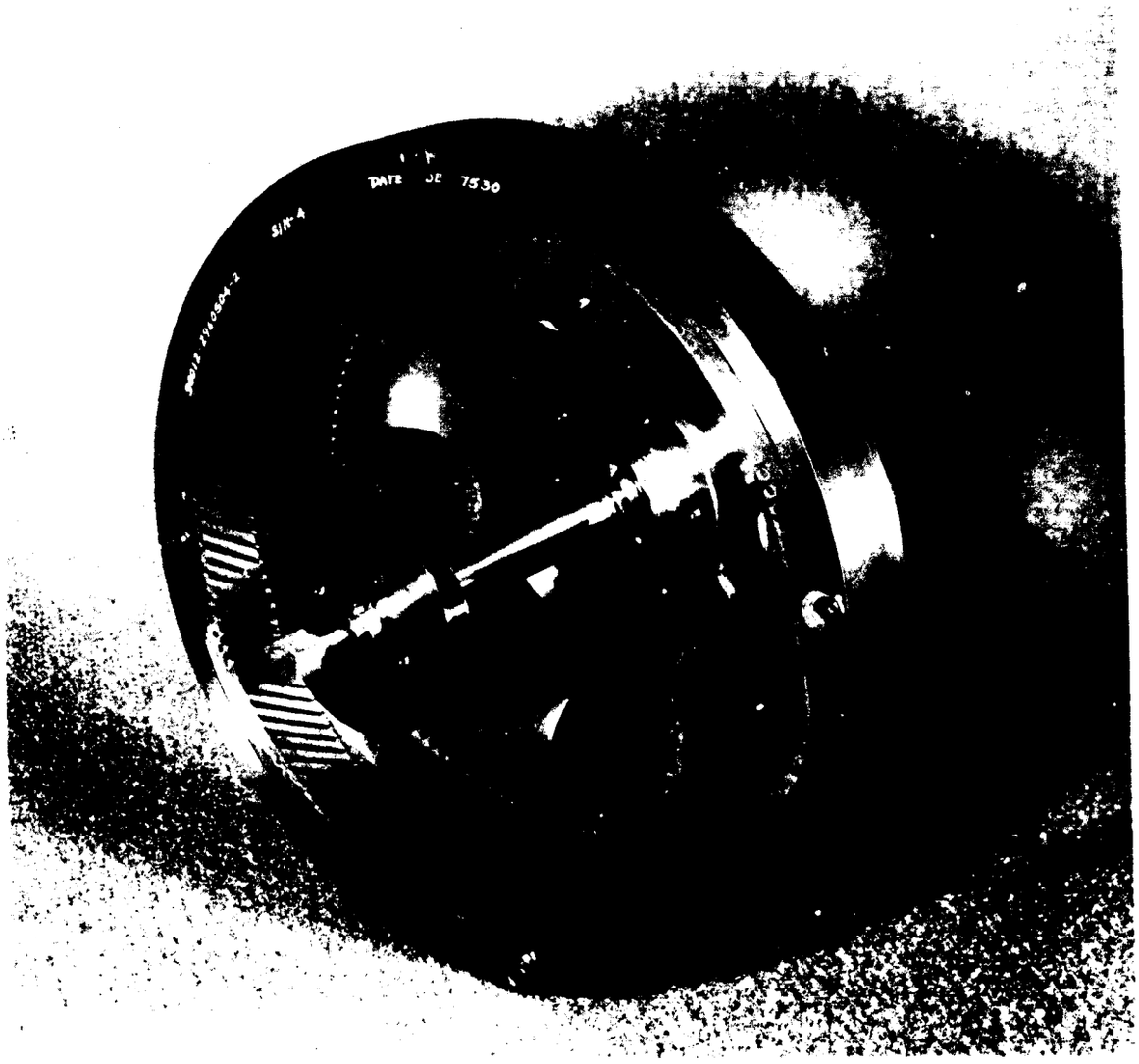

Figure 2-3
Rotor Assembly

Two machined parts form the rotor, the rim/web and shaft. They are thermally interference fitted together and bolted, and the motor cage is in turn thermally fit into the rim. The shaft design is such that all other parts of the rotor assembly can be assembled on the shaft from one end. The lower magnetic bearing rotor mounts on the shaft through a disk support; use of this support prevents direct clamping on the relatively soft magnetic bearing rotor, and also provides sensing surfaces for axial and radial position sensors. The radial sensors are mounted only for the purpose of rotor balancing, and are removed after balancing is complete.

b. Housing Assembly

The main structural component of the MBRW is the lower housing. It provides mounting for motor and tachometer components, forms part of the vacuum enclosure (required for performance testing in vacuum) and has mounting provisions (3 pads) at its outer diameter. The lower housing is a single part consisting of a conical web, with two concentric inner cylinders joined by four ribs. The inner cylinder provides mounting for the magnetic bearing stators and the lower touchdown bearings, and the outer cylinder provides mounting for the motor stator segments and tachometer probes. The motor stator segments are positioned axially by two shoulders on the outer cylinder of the lower housing, and are held radially by clamps which also serve as supports for the tachometer probes. This arrangement is best seen in Figure 2-4.

The tachometer probe mounting arrangement allows radial and tangential adjustment. The radial adjustment is required to set the nominal probe to tooth distance and the tangential adjustment is necessary to adjust the phase of one probe of the tachometer with respect to the other.

The upper housing partially encloses the unit and holds the upper touchdown bearings. An assembly machining operation of the upper and lower housing parts aligns the upper and lower touchdown bearings to the spin axis. Circumferential ribs in the upper housing are used to prevent local buckling of the shell under atmospheric pressure.

The lower cover completes the enclosure of the MBRW. It contains a port which is used for evacuation and is sealed by a plug. O-ring seals are used between all parts which comprise the MBRW enclosure.

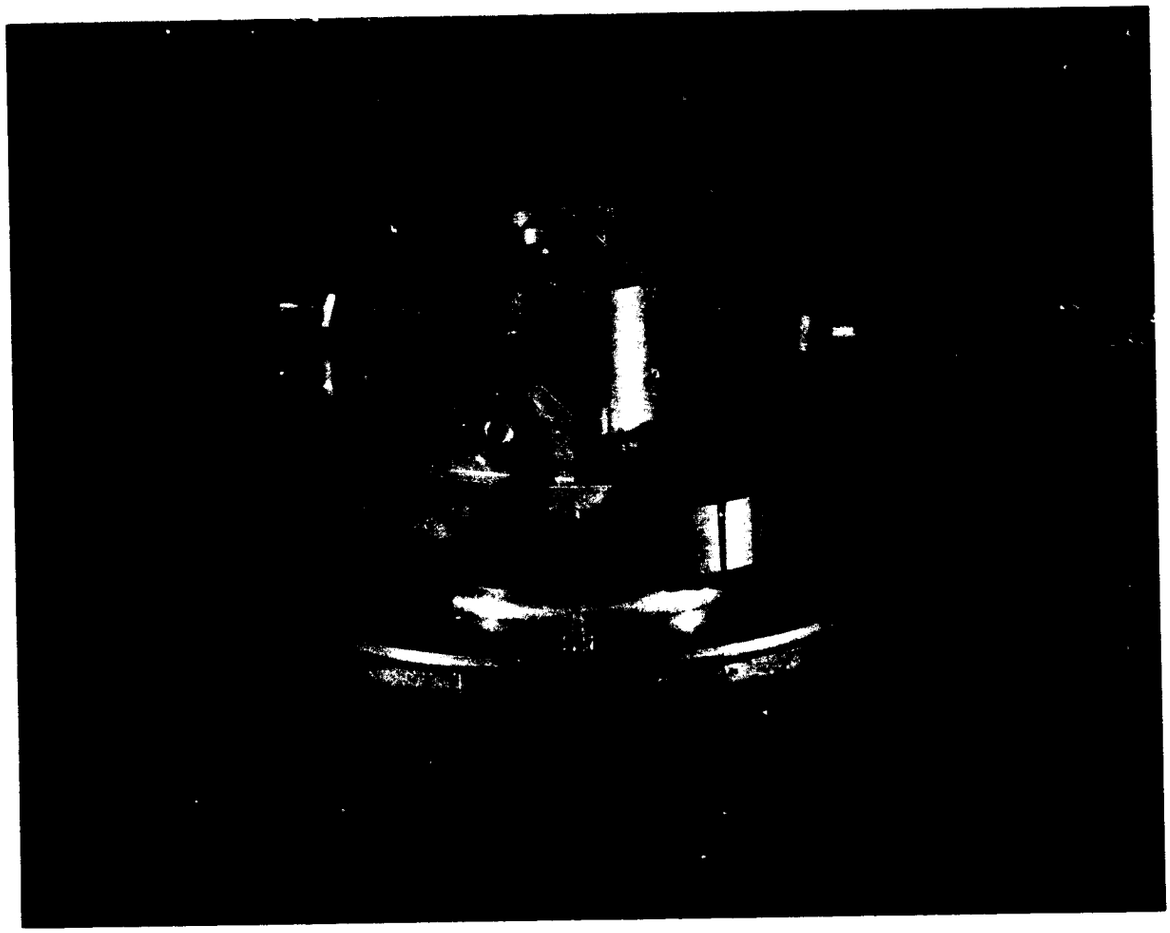

716 5 31

Figure 2-4
Lower Housing Assembly

The semicircular electronics boards are mounted on the lower housing. Each one contains the electronics for three proximity sensors, motor wiring connections and a connector. Separate headers are provided for the wiring of each channel, and the signal and power wiring for each channel has its own header for a total of four hermetc headers in the lower housing. All motor lead wires are brought through the headers to the boards where connections can be made to suit the drive scheme and voltage.

c. Spin Motor

The spin motor used in the MBRW is a two-phase ac induction motor. It consists of a single motor rotor (cage) and a redundant, segmented stator. Each motor channel consists of two diametrically opposed stator segments, each spanning 40 degrees of arc. The full stator circumference is equivalent to 32 poles. Each phase on a stator segment consists of two separate windings in order that the motor may be either bifilar-connected and driven squarewave or driven sine-wave (with series or parallel connection). The windings from the two segments can further be connected in either series or parallel. Operation in the various connections implies changing the drive voltage for a fixed-motor torque; the torque/power ratio is unchanged.

The motor cage consists of slotted laminations, axially stacked. Copper bars are inserted in the slots and are soldered to the copper end rings. The motor is designed to operate at a nominal radial gap of .024 inch. This relatively large gap, and the use of the diametrically opposed segments enables the achievement of low radial unbalance stiffness in the motor.

d. Touchdown Bearing System

A touchdown bearing system is provided to support the rotor, spinning or non-spinning, whenever the axial control system for the magnetic bearings is not operating. Duplex pairs of angular contact ball bearings are mounted in each housing half, outboard of the rotor. Nuts on the lower shaft provide shoulders which contact the inner races of the lower bearing pair and thereby limit axial motion in both directions. Shims between the shaft and the shaft end-nut allow the adjustment of the total shaft excursion. Shims between the lower bearing pair and the bearing support shoulder are used to center the bearings between the shoulders on the shaft assembly. A third shim adjustment is provided between the lower magnetic bearing stator and its supporting shoulder in the central tube of the lower housing.

This shim determines the size of the axial gaps between the magnetic bearing rotors and stators. No shoulders are used on the upper shaft so that deflection of the upper housing does not affect the touchdown system; this also simplifies assembly and adjustment of the touchdown bearing system.

The radial and axial gaps between the shaft and the touchdown bearing pairs are sized so that no contact occurs between any rotating and stationary parts when the magnetic suspension system is operating. Since the radial gaps determine both radial and angular travel, the span between the touchdown bearing pairs becomes important in limiting the angular travel.

The radial touchdown gaps are .010 inch; these touchdown gaps are the difference between the nominal tachometer gaps and the minimum worst case gaps. The axial touchdown gaps are set at ±.005 inch. These gaps are large enough so that when the rotor is at its equilibrium position in 1g with spin axis vertical, no contact occurs due to the offset of the rotor from its centered position. Larger axial touchdown gaps would necessitate increased currents and power at lift-off.

The touchdown bearings have radial and axial load capacities sufficient to prevent damage which would compromise their function. Since their function is quite different from spin bearings in a ball bearing reaction wheel (which is to spin continuously after a launch environmental exposure) different sizing criteria apply, i.e., higher static load levels can be tolerated without affecting performance. On the basis of an analysis of the environmental loadings, the MBRW touchdown bearings would be loaded to 145 percent of their thrust capacity and 50 percent of their radial capacity.

e. Materials

The material selected for the rotor web, rim and shaft is 6AL-4V titanium, based primarily on its thermal expansion coefficient being very nearly equal to that of the electrical iron of motor cage and magnetic bearing rotors. In addition, it is a stable material with high specific strength (strength-to-density ratio). The lower magnetic bearing rotor support is also titanium. The housing parts and cover are made of 6061 aluminum, but can be changed to a magnesium alloy in future units for weight reduction.

2.4 OPTIMIZATION AND SIZING

The objective of this optimization is to minimize the unit weight and meet the performance specifications within the constraints listed below. The design of Figure 2-2, evolved in the study, was used as a baseline, with the following constraints:

- Use of existing one-loop magnetic bearing design
- Use of existing segmented-stator ac induction motor design with redundant stator segments

The specifications which have a direct effect on the optimization are:

- Momentum: ±.5 ft-lb-sec
- Output torque — (a) .007 ft-lb, 4.2 watts
- Maximum input motor power — (b) .02 ft-lb, 12 watts

A computer program was used to calculate weights as a function of size (motor cage radius) and speed. Since the optimization result is not affected by component weights which are fixed, (e.g., electronics) these weights were not included in the weight calculation. The variable weights which are accounted for are those of the rotor assembly, the structure and enclosure. For reference, some computer runs were made in which the motor stator and cage were also considered variable within torque and power requirements. For these runs a 4 ounce-inch (.021 ft-lb) torque and 8 watt power were used since they are the nominal characteristics of the existing motor design.

The results of the optimization are shown in Figure 2-5. The constant weights have been included in these curves so that they show realistic MBRW values. These curves show that the size (3.5 inch radius) dictated by the use of the existing motor design is very nearly an optimum if operated at 700 rpm, and the use of this motor is not a severe restriction. Since this design point, 700 rpm, 3.5 inch radius, uses 8 watts and the specifications allow 12 watts, an extrapolation was made to use the full 12 watts and lighten the MBRW design. It was found that at 12 watts the speed is 1000 rpm and the unit weight decreases by .75 pound, indicating weight and power trade-off at about .2 pound per watt in this region. The final design point chosen was 700 rpm and 3.5 inch radius, that is, the heavier and lower power design; this choice was made because of the sensitivity to power in interplanetary applications. The final weight of the MBRW was 8.9 pounds (including estimated weight of flight-type redundant bearing electronics, but not including tachometer electronics) and a breakdown of this weight by component is shown in Table 2-2.

TABLE 2-2

MBRW COMPONENT WEIGHT SUMMARY

Component	Component Weight	Subassembly Weight	Assembly Weight
MBRW Total			8.9 lbs
Rotor Assembly		3.2	
Shaft	.09		
Rim-Web-Hub	1.74		
Magnetic Bearing Rotors (2)	.11		
Motor Cage	1.19		
Miscellaneous	.07		
Magnetic Bearing Stator Assembly (2)		1.34	
Iron Parts	.40		
Coil	.11		
Magnet	.12		
Spacer	.04		
Housing Assembly		4.0	
Lower Housing	1.26		
Upper Housing	.75		
Motor Stator (2)	1.36		
Cover	.21		
Tachometer Probe Supports	.13		
Touchdown Bearing Support	.11		
Tachometer Probes and Miscellaneous	.18		
Electronics Assembly (2)		.4	

2.5 MAGNETIC BEARINGS

The rationale for the selection of a dc magnetic, passive-radial, active-axial bearing system and the one-loop configuration was detailed in the design study Final Report, JPL Contract No. 953884. In such a system, the achievement of positive angular stiffness dictates the use of two radial-passive bearings with adequate axial spacing between them. The stabilizing torque of the bearing pair due to radial forces is thus made to exceed the destabilizing torque due to the axial unbalance forces.

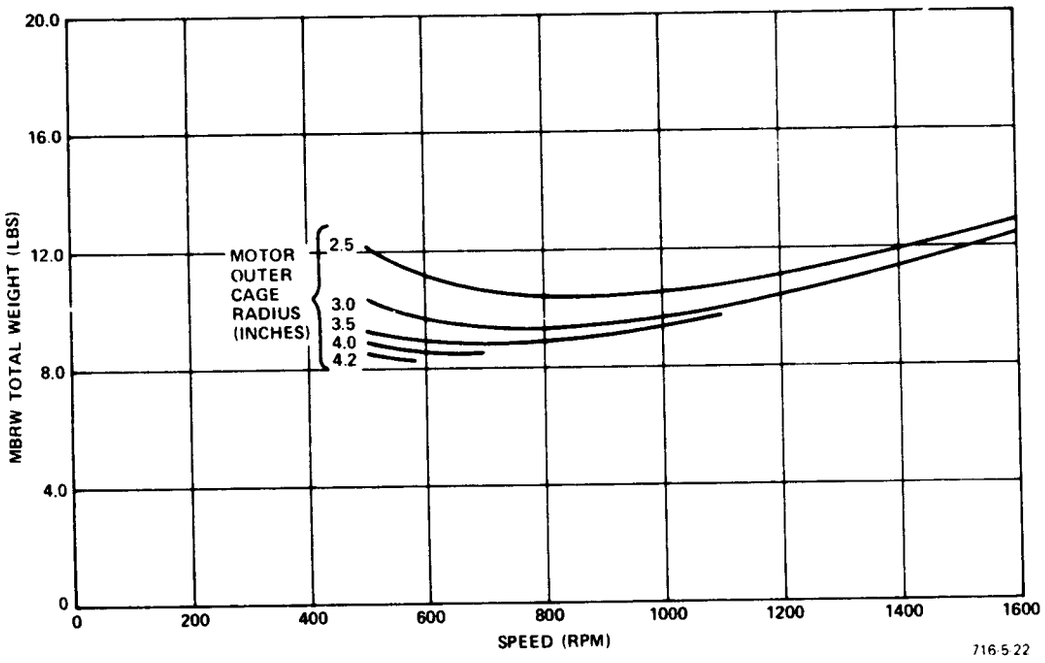

Figure 2-5
MBRW Weight as a Function of Speed and Size

The one-loop bearing system consists of a rotor and stator assembly at each end of the rotor shaft, as shown in Figure 2-6. The dc bias flux is provided by an axially magnetized ring magnet which is in series in the magnetic flux path. The control coil, which modulates the bias flux, is placed within the magnetic flux loop. A ring-groove geometry on the rotor and stator pole-pieces at the two air gaps is used to increase the radial stiffness.

The performance requirements for the MBRW primarily determine minimum radial and angular stiffnesses for the suspension system. The constraints are considered separately below. The mathematical constraint relationships were shown in the Design Study Report. Only numerical values are shown below.

a. Radial Capacity in a 1g Environment

The constraint on stiffness arises because of the requirement that the MBRW be capable of suspended operation at any speed, in any attitude, in a 1g environment and when subjected to a cross-axis rate of 35 milliradians per second.

$$K_{r1} \geqslant 35.7\ W_r$$

where

K_{r1} = required radial stiffness per bearing (lb/in.)

W_r = total rotor weight (lbs)

b. Radial Resonance Frequency $>$ 20 Hz

$$K_{r2} \geqslant 20.5\ W_r$$

where

K_{r2} = required radial stiffness per bearing (lb/in.)

c. Angular Resonance Frequency $>$ 20 Hz

$$K_{r3} \geqslant 80.2\ W_r$$

where

K_{r3} = required radial stiffness per bearing (lb/in.)

The above constraint assumes that the radial and angular stiffness are such that

$$K_\alpha = \frac{1}{4} K_r \ell^2$$

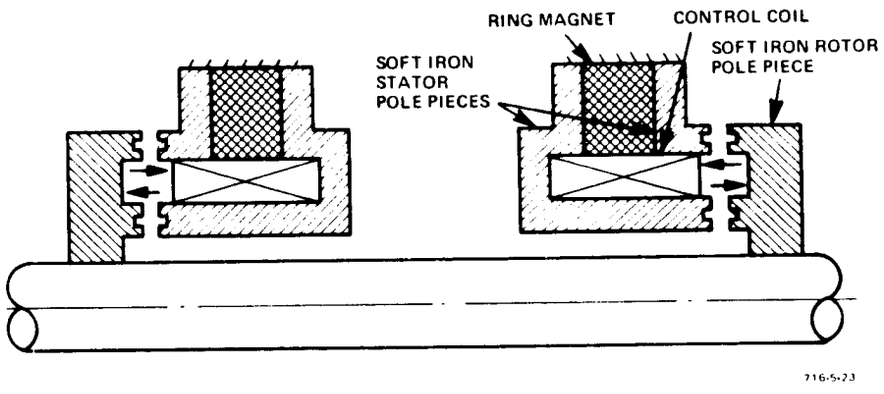

Figure 2-6
One-Loop Bearing System

where

K_α is the angular stiffness (in.-lb/radian)

K_r is the radial stiffness per bearing (lb/in.)

and ℓ is the axial separation between the two bearings, in inches.

d. Other Constraints

The cross-axis rate constraint dictates a radial stiffness of the order of only 10 lb/in.; the preliminary design indicated that the maximum operating speed would be $<$ 1200 rpm (20 Hz); hence no resonant conditions would be encountered in the nominal operating speed range.

The dominant constraint is seen to be that due to the angular resonance frequency. For a nominal rotor weight of 3 pounds, this indicates a required radial stiffness of K_r = 240 lbs/in. per bearing.

2.6 SUSPENSION CONTROL SYSTEM

The linear model of the magnetic suspension system used for preliminary design is shown in Figure 2-7. The suspension system is open-loop unstable (non-minimum phase) because of the negative static stiffness of the magnetics. The axial system is made stable by feedback control of the current through the control coils, based on a sensing of the axial displacement by the position sensor.

The simple linear system model shown departs from the actual system because:

- Structural compliance is not considered. Compliance in the rotor, stator or in the mounting modifies the system model, as typified by the analysis in Appendix B.
- In a one-loop bearing system, the control force/control current gain varies significantly with axial position because of the variation of gap flux density.
- Touchdown stops, power supply voltage and cross-over distortion in the amplifier are non-linearities in the actual system.

Several control schemes are possible. The concepts of two schemes were described in the Final Report, JPL Contract No. 953884. The scheme implemented in the MBRW is a lead-lag compensation with minor-loop integrator. The lead-lag

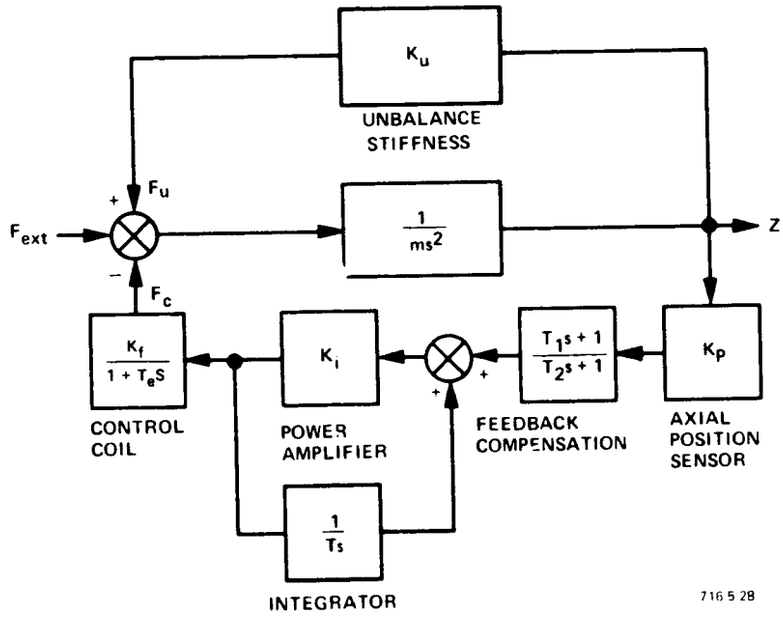

Figure 2-7
Linear System Model of Axial Control System

compensation may be thought of as position-rate feedback, and governs the fast axial dynamics. The addition of the relatively slow integrator enables zero-current operation under steady axial external loads e.g., in 1g when the MBRW is being operated with spin axis vertical. The static axial stiffness with the integrator is thus negative, the rotor being so positioned that the external force is exactly balanced by the unbalance force of the magnetics. The use of the integrator also maintains long-term zero-current operation regardless of drift in the electronics or the position sensor.

The root locus for the control system is shown in Figure 2-8. Preliminary design numbers used for the analysis are shown in the figure. It can be seen that the dominant pole is due to the integrator. Of the 3 other poles, at suitable values of loop gain, either the complex pair or the real pole can be made dominant by suitable placement of the lead and lag frequencies. It can be seen that for the root locus shown $K/K_u = 1.4$ will ensure that the damping coefficient $\geqslant .6$; the dominant real pole is in the region of -400 radians/sec, which will ensure a rise time $\leqslant 6$ msec. The dominant integrator pole is ≈ 75 radians/sec.

2.7 SUSPENSION ELECTRONICS

The function of the suspension electronics is to provide controlled coil currents, thus generating axial forces to lift-off and maintain levitation of the rotor. The main components, as shown in Figure 2-9, are the axial position probe and its driver, compensation network, power bridge, and an integrator. The primary design requirements are maximum reliability, axial stability of the rotor, and minimum power. Complete electronics redundancy is also required to prevent a single point failure; hence, there are two separate suspension electronics channels with their corresponding position sensors. Selecting suspension channels is accomplished at the front panel of the MBRW Electronics Assembly.

a. Position Sensors

The axial position of the rotor is measured by an eddy-circuit position sensor. The sensing element is a small diameter coil of wire that is excited by a high frequency (2 MHz) ac source. The radiated field of the coil sets up eddy-currents in the sensed surface. Variations of the probe-to-surface gap cause a variation of the probe impedance which changes the ac signal amplitude. This signal is then filtered to provide a dc voltage proportional to displacement (typically 250 volts/inch).

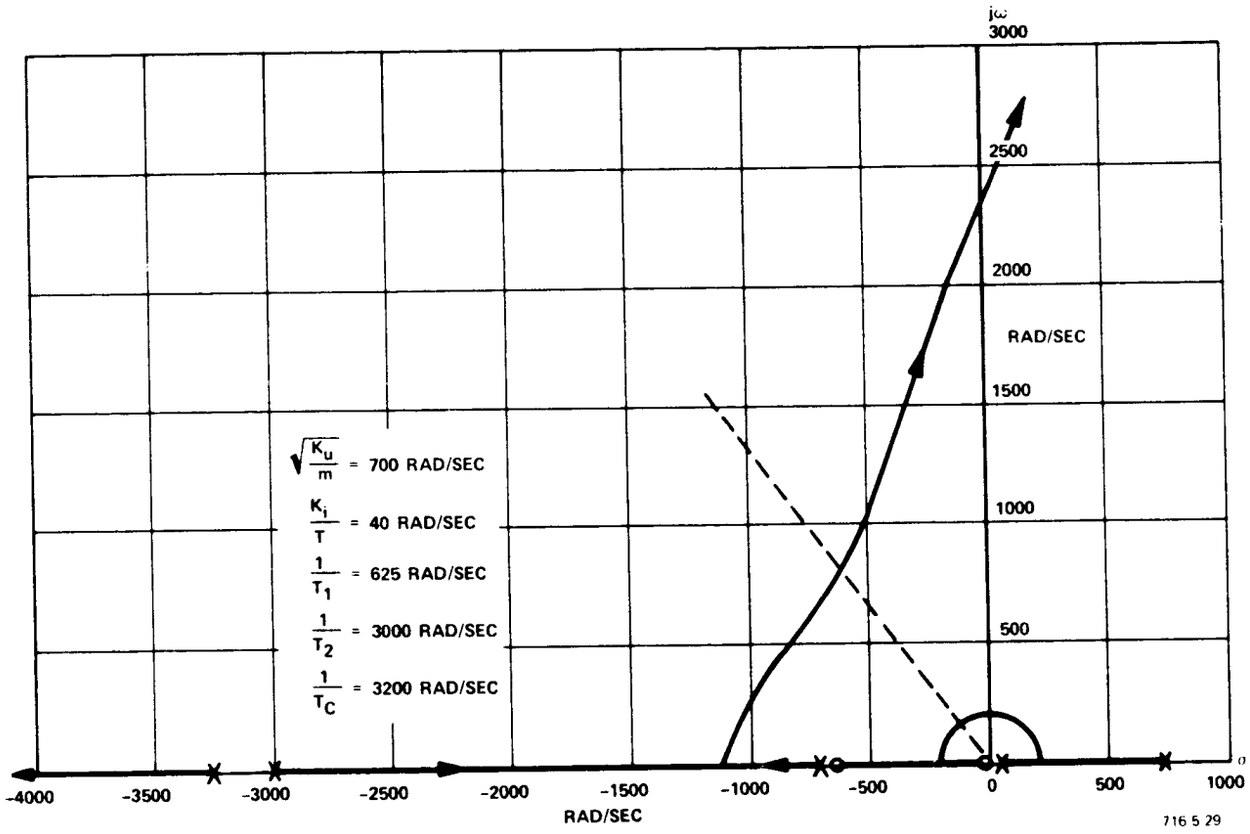

Figure 2-8
Root Locus, Axial Control System

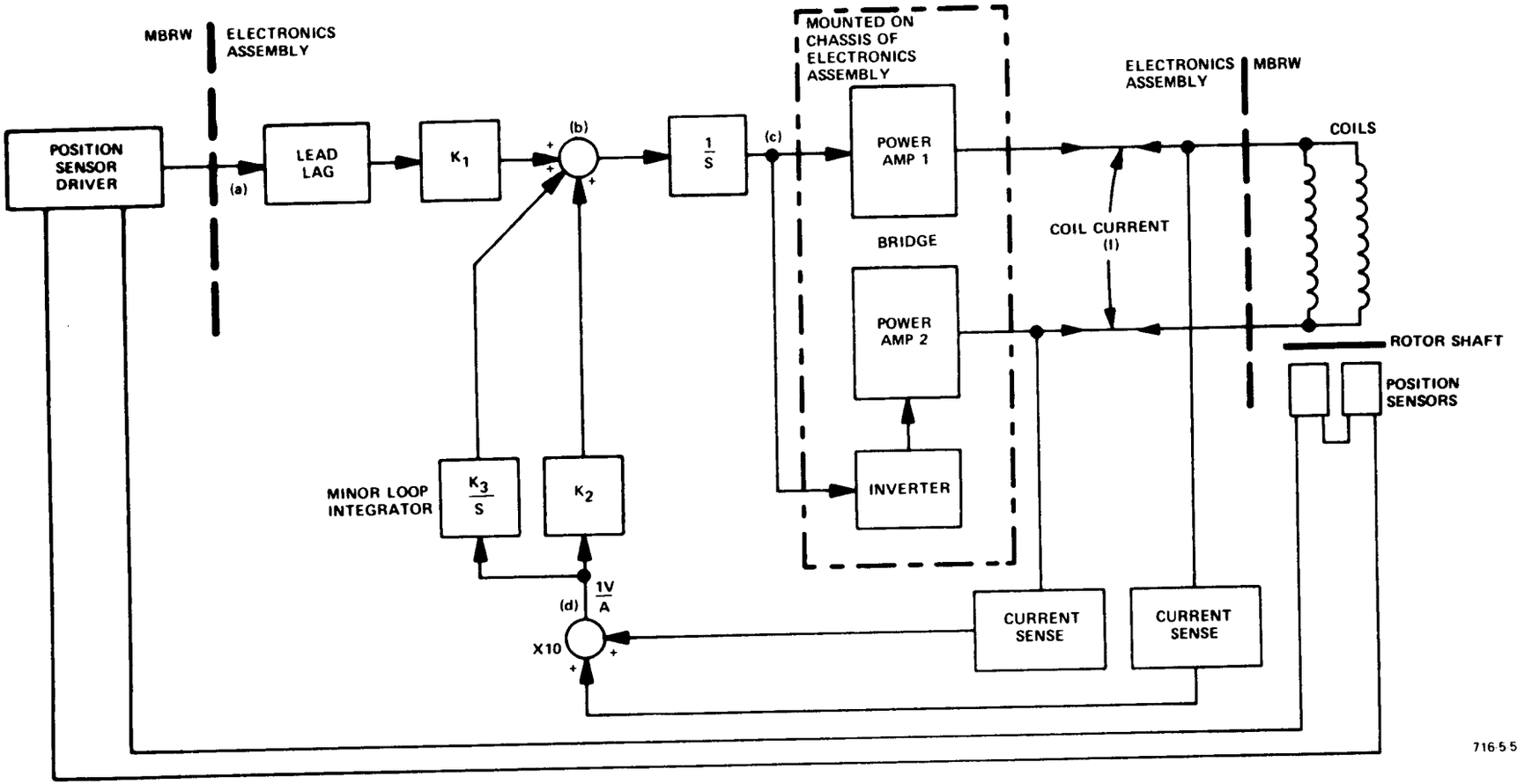

Figure 2-9
Suspension Electronics - Block Diagram (One of Two Channels)

The rotor displacement (z) was initially designed to be measured by a single eddy-current probe positioned .9 inches from the rotor spin axis as shown in Figure 2-10. However, the single position measurement allowed the angular component, $+ \Delta z$, of rotor movement to be coupled into the axial measuring system, thereby creating an instability in the suspension electronics. This problem was corrected by the addition of another probe at the same radius 180 degrees away, as shown in Figure 2-11. The angular component Δz due to θ is now removed (P_1 measures $a - \Delta z$ and P_2 $a + \Delta z$) leaving only the axial component. Series connection of the probes simplified the electronics by eliminating the need for an extra probe driver and output summation circuitry; however, exact cancellation of the angular component was not possible since the gains of the series-connected probes could not be individually adjusted. The ultimate solution for this problem is to use an annular ring probe which averages the probe to rotor gap thereby eliminating angular variations. Initial development tests on such a probe at Sperry have confirmed the feasibility of the approach.

b. Compensation

Compensation consists of a single lead/lag network (Figure 2-9). The gains K_1 and K_2 and the phase lead are adjusted such that the phase curve is above -180 degrees (phase margin) at zero dB gain crossover. This keeps the gain below zero dB when the phase curve is below -180 degrees (gain margin). Adequate gain and phase margin (> 5 dB, $> 10°$) ensures axial stability. The lag is adjusted to prevent structural resonances from affecting stability of the axial system by attenuating the high frequency gain.

The integrator is used, with positive feedback, to minimize steady-state power consumption under steady external loads, and to eliminate the effects of electronic component and position sensor drift over time and temperature. Steady-state coil currents are integrated and added to the compensated position signal. The rotor is thus axially repositioned to a point at which the rotor is at a force equilibrium, with the permanent magnet forces exactly balancing the steady external axial forces. At this point no coil current is required.

c. Power Amplifier

The power amplifier consists of a linear power bridge which controls current in either direction (with power amplifiers 1 and 2, Figure 2-9) through the parallel coils in response to the compensated signal from the position sensor.

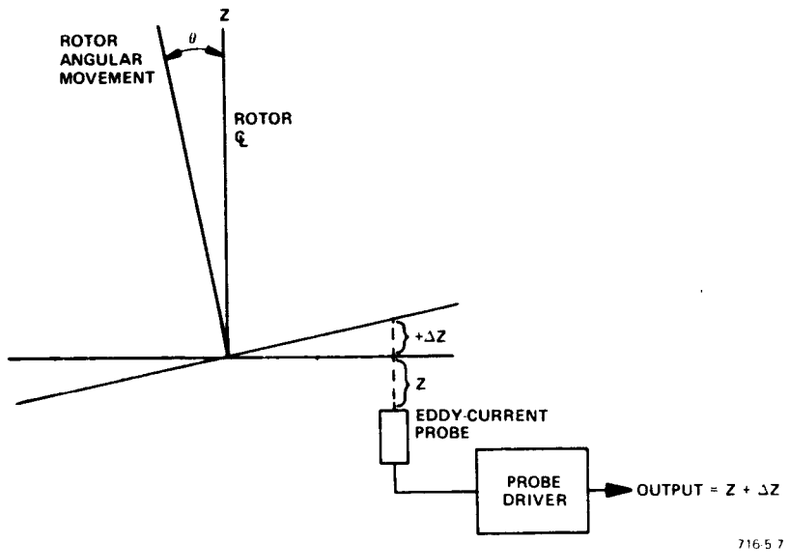

Figure 2-10
Rotor Sensing with Single Position Sensor

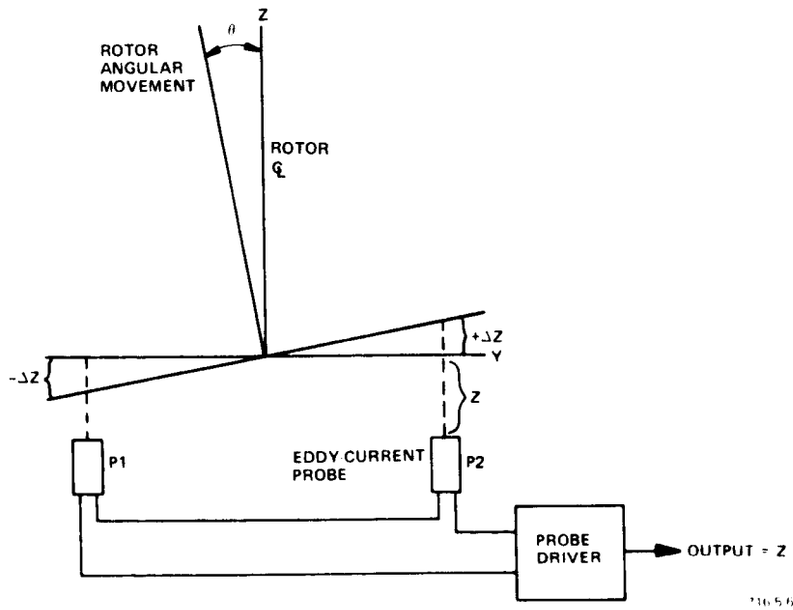

Figure 2-11
Rotor Sensing with Series Connected Position Sensors

An undesirable characteristic of power bridge circuits is crossover distortion. Before either power amplifier will fully conduct, about +1.2 volts (two) transistor drops) must be present at point c in Figure 2-9. This creates a deadband of 2.4 volts about the coil current axis as shown in Figure 2-12. The coil current to voltage gain is lower in this region causing limit-cycle oscillations. Adding a dc bias voltage of +2.4 volts at power amplifier 1 removes the deadband by biasing both the power amplifiers just to the point of conduction as shown in Figure 2-13. Adequate gain for axial stability is now available for all values of input voltage. The biasing entails a standby power of .25 watt.

Both channels of control electronics are mounted on circuit board cards which are located in the Electronics Assembly chassis. The power bridges are mounted on the chassis for heat sinking. The position probes are internally mounted in the MBRW. The high frequency ac drivers for the probes are mounted on metal cards on the underside of the MBRW. The gain of the position sensor is dependent on the cable length between the probe and its driver; the driver location on the underside of the MBRW keeps this cable length short which allows more gain and bias voltage variation with gap.

2.8 TACHOMETER

Design requirements for the tachometer were a minimum of 360 pulses per revolution and a direction of rotation indication. Employing two specially fabricated eddy-current probes to sense 130 teeth, machined on the inside of the umbrella rotor, (see Figure 2-14), the tachometer provides 520 pulses per revolution for speed indication of rotation output. Speed insensitivity of the eddy-current probes allows accurate indication of rotor speed and direction of rotation through 0 rpm. The number of teeth (130) were chosen on the basis of probe sensitivity and minimum operating tachometer/probe gap.

The eddy current tachometer sensor was chosen over three other methods:

1. Optical encoder disk
2. Coaxial light source and detector
3. Hall effect sensor

In each of the other methods, reliability and lifetime of the sensors was unknown for a 10-year period. In addition, the Optical Encoder Disk and the Hall Effect Sensor require extra components in the form of an inscribed glass disk and an external magnetic circuit, respectively. Previous experience with the eddy-current

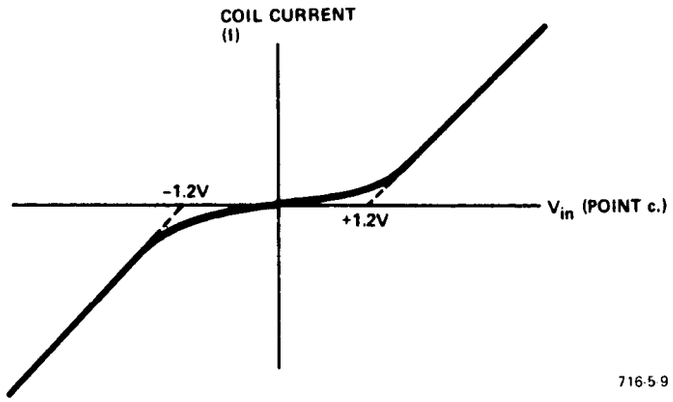

Figure 2-12
Power Bridge Voltage Deadband

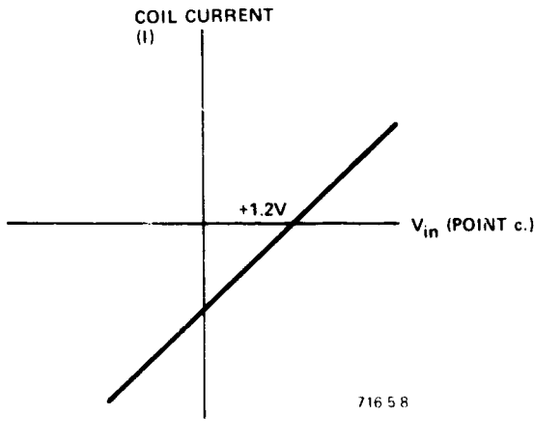

Figure 2-13
Power Bridge Characteristic After Elimination of Deadband by Biasing

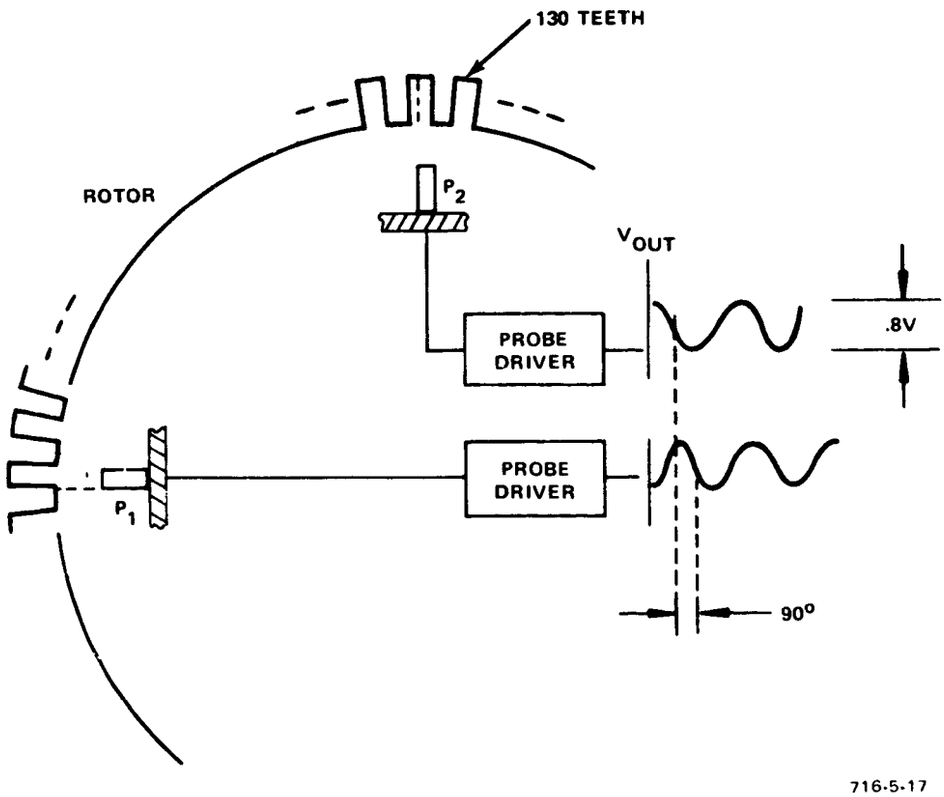

Figure 2-14
Tachometer Probe Arrangement (One of Two Channels)

probe has found it to be the simplest, cheapest, smallest and most reliable sensor of the four. In addition, the sensor drive circuits are the same as those used for the axial position sensors.

The probe driver outputs are sine waves which are processed by high gain amplifiers into TTL compatible (0 to +5 volts) squarewaves (see Figure 2-15(a)). The squarewave corresponding to each probe is then fed to a positive and negative edge triggered one-shot whose output is a 40 microsecond pulse corresponding to the leading and trailing edges of the input squarewaves. One-shot operation is illustrated in Figure 2-15(b). Hence, each probe output is converted to 260 pulses per revolution or twice the number of teeth. The pulses from the two probes are then summed, giving 520 pulses per revolution (4 times number of teeth). A dc level scaled to 1 volt/100 rpm is obtained by lowpass filtering the pulse train.

To obtain direction of rotation, a digital latch determines the relative phasing of the tachometer probes and provides an output in the form of a discrete dc level.

Accurate speed and direction of rotation information through 0 rpm is provided, resulting in a smooth transition of data from one direction to another with virtually no deadband. A self-biasing network was also designed to compensate for power supply drift, component aging, and rotor runout by maintaining a constant switching point of the high gain amplifier on the probe waveform. This circuit ensures accurate speed information over temperature and time.

The probes are placed 90 mechanical degrees apart to minimize effects due to rotor whirling. The probe drivers are mounted to the underside of the MBRW, similar to the axial probe drivers. The tachometer electronics are circuit board mounted (1 channel per board) and are located in the Electronics Assembly. Tachometer monitoring and channel select is accessible in the tachometer section at the front panel of the Electronics Assembly.

2.9 MONITORING ELECTRONICS

The MBRW Electronics Assembly processes signals from the MBRW to provide indication of rotor levitation, rotor speed, and direction of rotation. A cautionary indication of rotor overspeed is also provided. Figure 2-16 shows the monitoring and indicating functions.

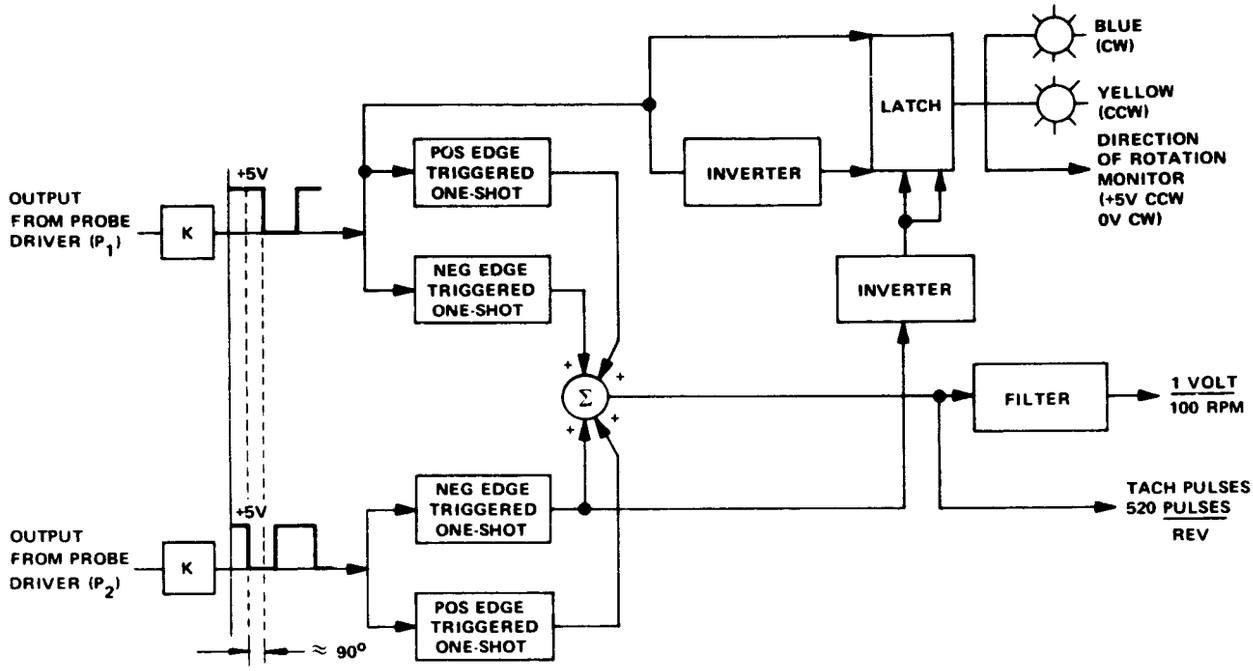

Figure 2-15a
Tachometer Electronics Block Diagram (One of Two Channels)

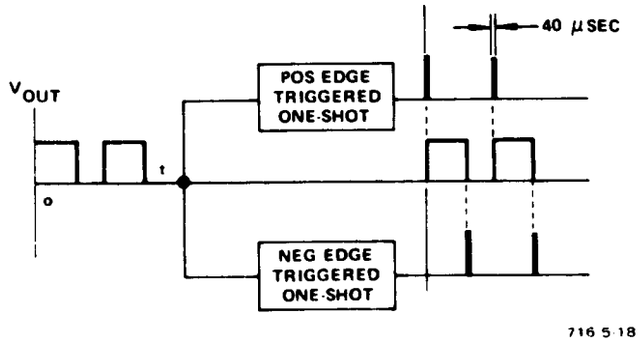

Figure 2-15b
One-Shot Operation

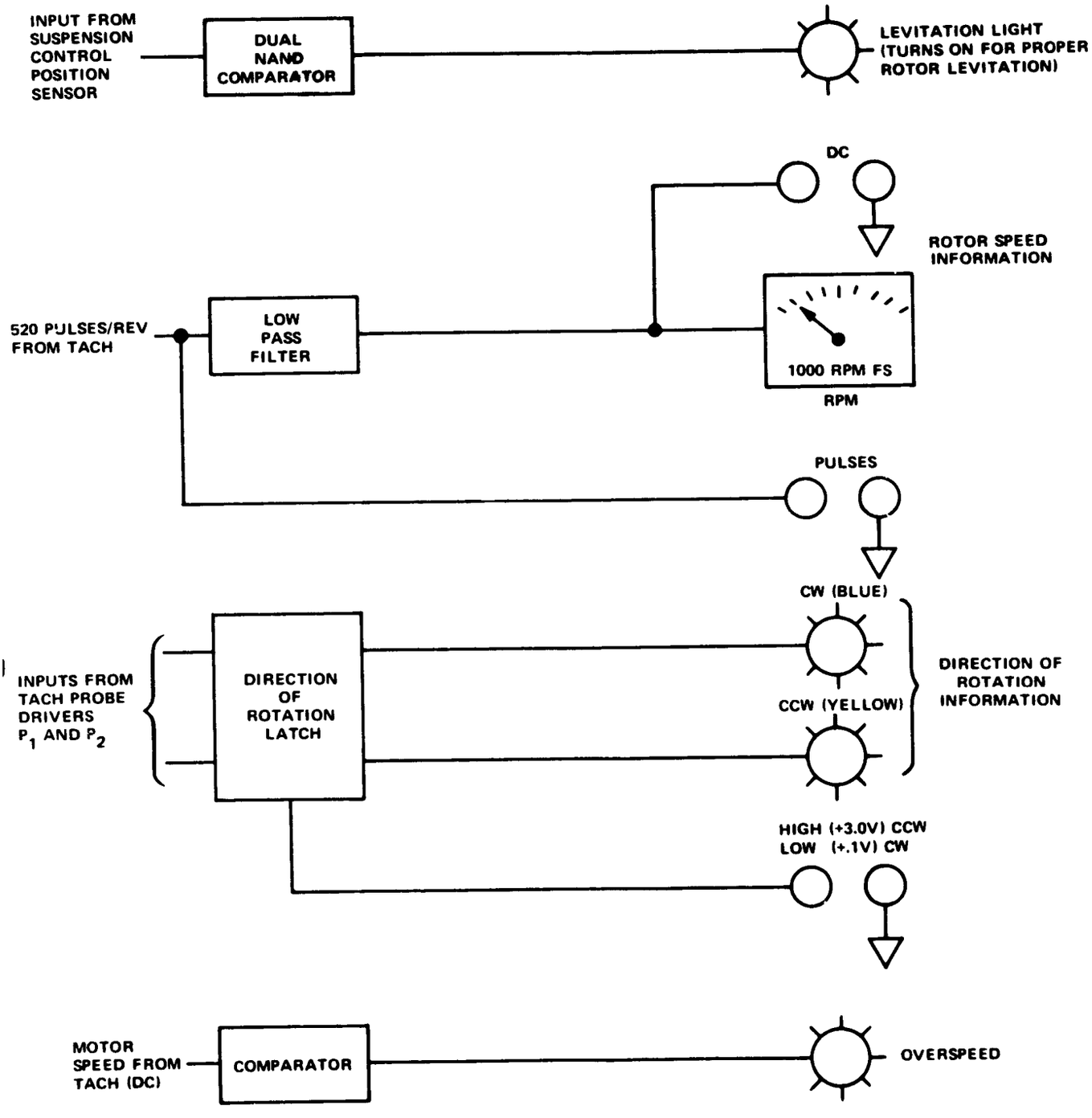

Figure 2-16
Monitoring Electronics Block Diagram

a. Rotor Levitation

Proper magnetic suspension of the rotor turns on a green light in the Bearing Control section. The dc voltage output from the suspension position sensor is nominally +7.3 volts with rotor leviated, +5.6 volts and +8.2 volts when the rotor is on its lower and upper touchdown bearings respectively. A dc bias of +6.8 volts and +7.8 volts is set on two comparators. The output of each comparator is tied to the positive side of a diode with the negative side of both diodes tied together. Thus, rotor levitation triggers both comparators, turning on the levitation light.

b. Rotor Overspeed

At a rotor speed of 750 rpm, the overspeed light in the Spin Motor Control section comes on. This warning is used to indicate the speed at which the tachometer output becomes erroneous due to one-shot pulse overlapping. Care should be exercised in operating at speeds beyond 750 rpm because of erroneous rotor speed indication.

c. Rotor Speed Readouts

Rotor speed information is provided in two forms:

1. Pulses - 520 pulses per revolution
2. DC - 1 volt/100 rpm

The pulse output in the Tachometer section is from a 4-input nand gate in the Tachometer Electronics which sums the one-shot outputs from both tachometer probes. These pulses are also sent through a low pass filter for driving a front panel dc voltmeter at 1 volt/100 rpm. This dc voltage is also available for output to an external monitoring device, e.g., a chart recorder.

d. Direction of Rotation Readouts

A digital latch in the tachometer measures the relative phase difference between both tachometer probe signals to determine the direction of rotation of the rotor. The latch drives front panel lights to indicate direction of rotation: blue - Clockwise (CW), yellow - Counterclockwise (CCW). A discrete dc level (+3 volts counterclockwise, +.1 volt clockwise) is also provided for monitoring.

2.10 RELIABILITY

Redundancy specifications (no single-point failure) of the MBRW requires two completely independent channels, with each channel consisting of tachometer and suspension electronics and a segmented induction motor. The calculated reliability is required to be .98 for 10 year operation. To achieve maximum reliability, each section is assumed to be independently switched between channels (see Figure 2-17) when a failure is detected. Switching of the entire channel in case of a failure in a particular section is another method but produces lower reliability.

Reliability Analysis:

$$R_{S_T} = 1 - \lambda S^2 \cdot t^2 = \text{total parallel reliability of both suspension electronics channels}$$

$$R_{TA_T} = 1 - \lambda TA^2 \cdot t^2 = \text{total parallel reliability of both tachometer electronics channels}$$

$$R_{M_T} = 1 - \lambda M^2 \cdot t^2 = \text{total parallel reliability of both motor channels}$$

where

λS = number of failures of single suspension electronics channel per hour

λTA = number of failures of single tachometer electronics channel per hour

λM = number of failures of segmented induction motor per hour

and

t = desired operating time (87.6×10^3 hour, or 10 years)

The total reliability is

$$R_{total} = R_{S_T} \cdot R_{TA_T} \cdot R_{M_T}$$

$$\approx 1 - t^2 (\lambda S^2 + \lambda M^2 + \lambda TA^2)$$

where the calculated failure rates used, assuming high-reliability components were

$\lambda S = .7022 \times 10^{-6}$ per hour

$\lambda TA = .2839 \times 10^{-6}$ per hour

$\lambda M = .0012 \times 10^{-6}$ per hour

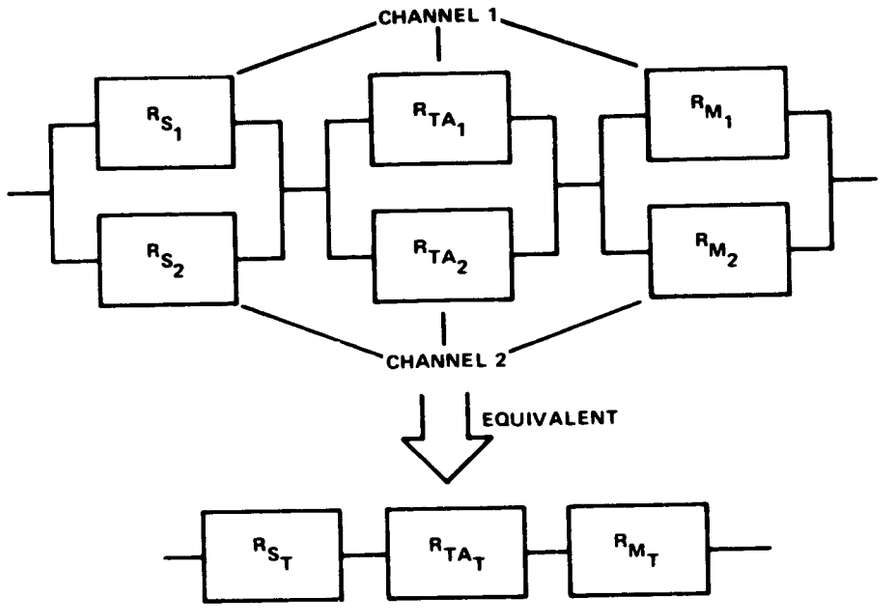

WHERE R_S = RELIABILITY OF SUSPENSION ELECTRONICS

R_{TA} = RELIABILITY OF TACHOMETER ELECTRONICS

R_M = RELIABILITY OF SEGMENTED INDUCTION MOTOR

716-5-15

Figure 2-17
MBRW Reliability Model

The above failure rates were determined on the basis of the electronics part lists shown in Tables 2-3 and 2-4.

Substitution of the numerical values indicates that the calculated reliability is .995 for a 10 year life. For comparison, if it is assumed that the motor, suspension and tachometer are not independently switched, the calculated reliability is .992.

TABLE 2-3

ELECTRONICS PARTS LIST FOR JPL MBRW

A. Suspension Electronics (one of two channels) includes position sensor drivers.

Quantity	Description	Manufacturer	Status
4	Op-Amps (LM108A)	National	APL
2	Power Transistors (SDT 3303)	Solitron	APL
2	Power Transistors (2N 3997)	T.I.	PPL
2	Transistors (2N 3501)	Mot	PPL
2	Transistors (2N 2907A)	T.I.	APL
30	Metal Film Resistors (.5%)	IRC	APL
6	Diodes (IN4148)	GEC	APL
4	Power Diodes (IN5417)	Semtech	PPL
2	Resistors (3 watt wirewound)	Dale	APL
12	Capacitors (Ceramic)	Aerovox	APL

Miscellaneous

2	Eddy Current Probes	- Bently Nevada (Part No. 190-F)
1	Segmented Induction Motor	- Sperry Electro Components Part No. 5100-10415A
1	Control Coil	- Sperry Part No. 5100-30564

TABLE 2-4

ELECTRONICS PARTS LIST FOR JPL MBRW

B. Tachometer Electronics (one of two channels) includes position sensor drivers.

Quantity	Description	Manufacturer	Status
4	One Shot (54L121)(1)	T.I.	PPL
2	Op-Amp (LM101A)	National	APL
2	Transistors (2N2222A)	T.I.	APL
1	4-Input Nand (7420)(2)	National	
1	2-Input Nand (74L00)(3)	T.I.	
18	Resistors (Carbon) (5.0%)	ABC	APL
16	Resistors (Metal Film) (.5%)	IRC	APL
16	Capacitors (Ceramic)	AVX	APL
2	Capacitors (Electrolytic)	SPR	APL
4	Transistors (2N2907A)	T.I.	APL

(1) Substituted on breadboard electronics due to unavailability of T.I. 54L122 (APL) because of lead time.

(2) Used on breadboard only. Signetics 5420 (APL) will be used for flight.

(3) Used on breadboard only. T.I. 54L00 (APL) will be used for flight.

Miscellaneous

2 Eddy Current Probes - Bently Nevada Part No. 070-F)

SECTION 3.0

MBRW CALIBRATION AND TEST RESULTS

SECTION 3.0

MBRW CALIBRATION AND TEST RESULTS

3.1 ROTOR AND SUSPENSION SYSTEM CHARACTERISTICS

Measurements were made of the suspension system characteristics and are summarized in Table 3-1. The radial, angular and unbalance stiffness values were measured by direct loading and the angular and radial values were verified through measurement of their natural frequencies. Damping ratios were determined by observation of the decay of angular and radial motions.

It was found that angular stiffness was considerably below that required to maintain the angular natural frequency above 20 Hz as required. The radial stiffness was also about 75 percent of the desired value. This combination, together with the axially offset center of gravity of the rotor, allowed touchdown of rotor on the touchdown bearings with the spin axis horizontal.

The low angular stiffness was due to the relationship relating angular stiffness to radial stiffness as a function of geometry (bearing span to radius ratio and ring placement) being more complicated than prior experience had indicated. The angular stiffness thus has a destabilizing term related to the axial unbalance stiffness.

Solution of the problem will involve placement of the rotor c.g. at the bearing midspan, a possible decrease of the gaps of the magnetic bearing and experimental confirmation of the relationship between angular, radial and axial stiffness.

Testing of the MBRW confirms that the first critical speed is well above the 700 rpm operating speed and occurs at approximately 1770 rpm. Due to the low radial damping coefficient (.01) of the magnetic bearing system, the motion becomes quite large at this critical speed.

Balancing was carried out using displacement information from each shaft end to determine required balance corrections. Details of the method used are given in Appendix A. This method accounts for the various non-symmetries of the rotor, suspension and correction planes, and allows simultaneous corrections of the static and dynamic unbalance. The initial static and dynamic unbalances were .12 oz-in. and .13 oz-in.^{2}, respectively, and the final levels were calculated to be .0035 oz-in. and .019 oz-in.^{2}. With unbalances of these levels the operation of the

TABLE 3-1

ROTOR AND SUSPENSION SYSTEM CHARACTERISTICS

Stiffness Values		
Radial (total)	295	lb/in
Angular	125	in-lb-rad
Unbalance (total)	2750	lb/in.
Damping Ratios		
Radial	.01	
Angular	.22	
Natural Frequencies		
Radial	29	Hz
Angular (zero speed)	9	Hz

MBRW at 700 rpm was quite smooth. Mass removals for balance corrections were made without removing the rotor from the housing and without disturbing any of the parts of the rotor.

Tests were made to determine the effect of motor radial unbalance forces on rotor motions. The motor was driven so that the output torque was at least 4 oz-in. Some effects on the shaft motions could be seen, but these effects were a fraction of the residual unbalance effects.

The function and integrity of the touchdown bearing system were verified by deactivating the control system at zero speed, at half speed and at the maximum speed of 700 rpm. This test was done 100 times at zero speed, 25 at 400 rpm and 25 at 700 rpm. No changes in the function or alignment of the touchdown system were observed. Touchdown and relevitation produced no noticeable changes in balance.

3.2 CONTROL SYSTEM PERFORMANCE

a. Compensated Open Loop Gain and Phase Response

The open loop response curves were arrived at by connecting a signal generator to point (b) in Figure 2-9. The amplitudes of the signals at points (a) and (b)

were then measured as a function of the input frequency. The amplitude at (b) was maintained at 20 mv (peak-peak) over frequency to remove nonlinear effects in the power bridge. The left vertical axis of the open-loop response curves represents gain (20 log Va/Vb) in 5 dB steps. The right vertical axis is the phase difference between points (a) and (b) expressed in degrees.

The MBRW was designed to be mounted at three tabs spaced 120 degrees apart at the OD of the lower housing. However, a structural resonance in the region of 200 to 300 Hz was identified as being due to the web compliance of the lower housing. The open-loop gain and phase response for this mounting is shown in Figure 3-1. Phase and gain crossover occur very close together, thereby implying a marginally stable axial system. A single lead/lag for compensation, with the lead at 75 Hz and the lag at 350 Hz, does not provide adequate gain and phase margins with this mounting.

The structural mode due to the web compliance was completely eliminated by bypassing the web compliance of the lower housing (Figure 3-2). The MBRW is mounted with six 3.5 inch posts attached at the ID of the position sensor driver boards on the underside of the MBRW. The posts are then mounted to a large metal plate for rigidity. The web resonance at 280 Hz was eliminated with adequate gain and phase margin for axial stability. When the plate is mounted to a massive structure (heavy lab bench, floor-mounted pedestal, etc) the open-loop response approaches that of a rigid body. The compliance of the web can be easily eliminated in future designs by thickening of the conical web at an estimated weight increase of .1 pound. The rotor web resonance occurs at 1800 Hz. Because of the 40 dB/decade roll-off, this structural resonance is adequately gain-compensated and is not shown on the response plots.

b. Lift-Off and Operating Current

Coil current is measured at the output of the summation amplifier in Figure 2-9. The signal at point (d) is scaled at 1 volt/ampere. Figures 3-3 and 3-4 are composite photographs of coil current and rotor position when the rotor is closest to and farthest away from the position sensors prior to lift-off, with the MBRW spin axis vertical.

	Peak Current	Peak Power
Rotor traveling away from sensors (up)	1.4 amperes	39.2 watts
Rotor traveling towards sensors (down)	.7 ampere	19.6 watts

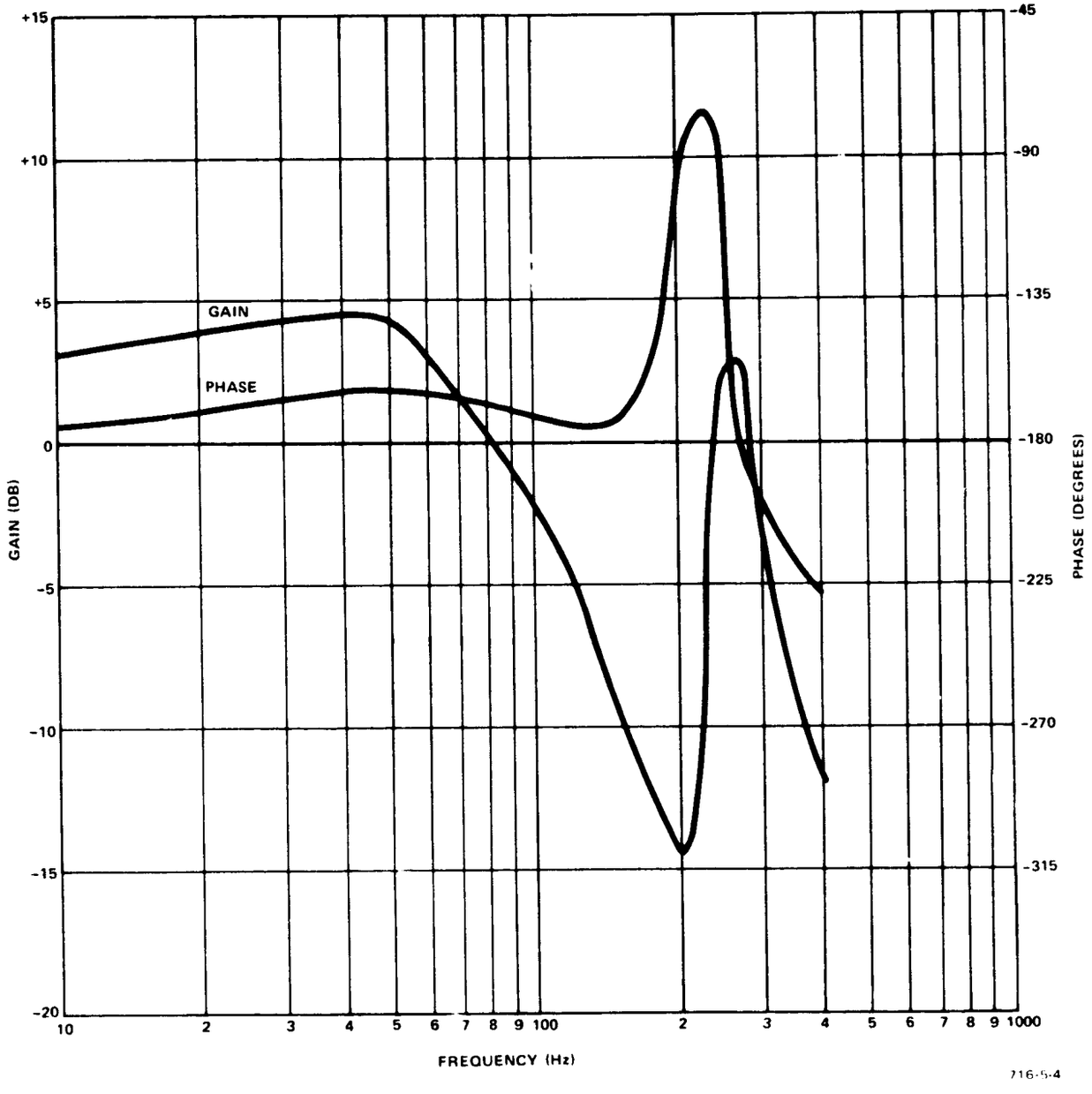

Figure 3-1
Compensated Open-Loop Gain and Phase
Response Showing Effect of Web Compliance

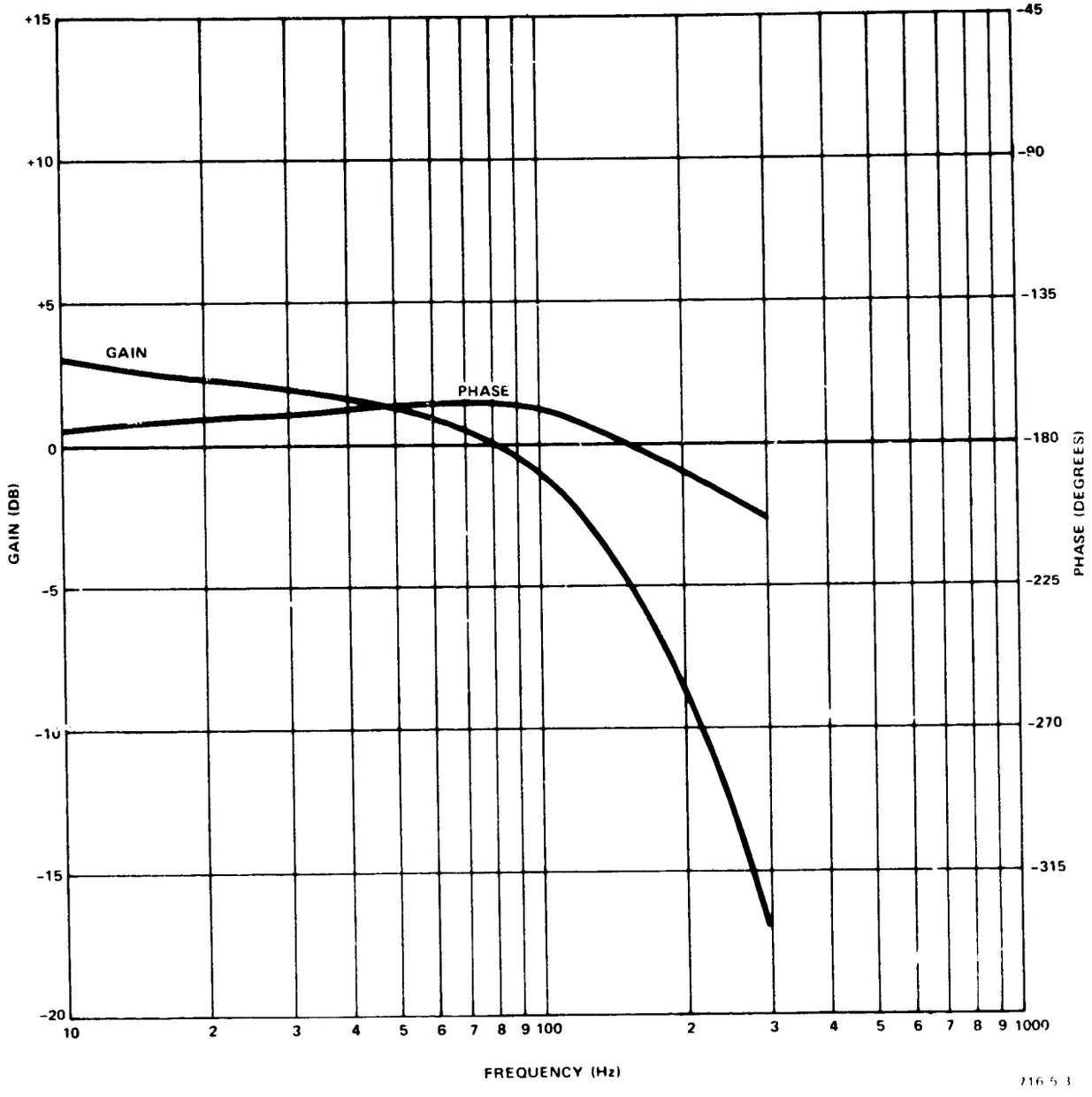

Figure 3-2
Compensated Open-Loop Gain and
Phase Response Without Web Compliance

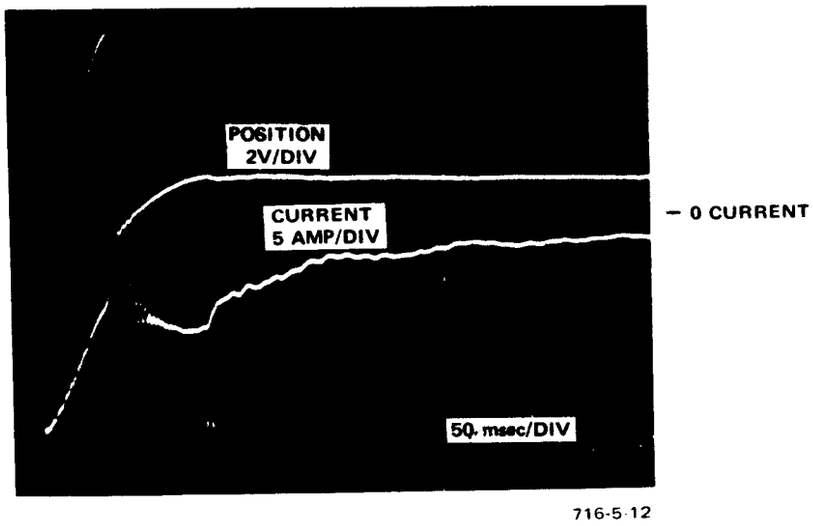

Figure 3-3
Coil Current and Rotor Position at Lift Off
(Rotor Traveling away from Position Sensors)

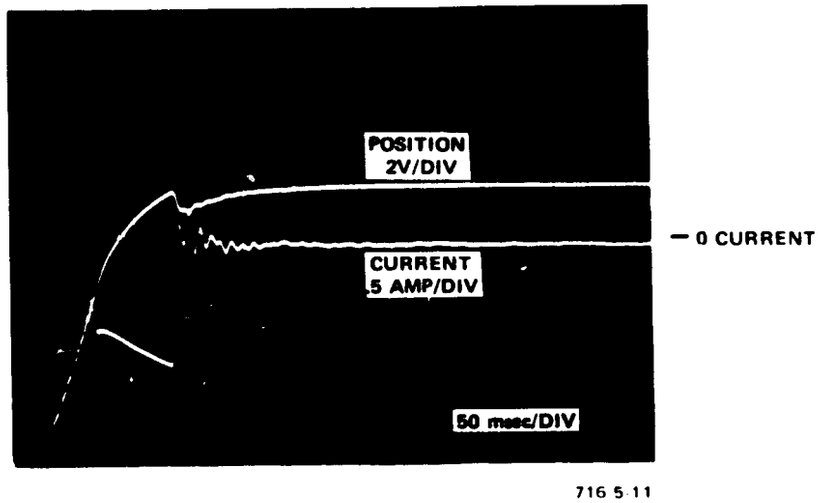

Figure 3-4
Coil Current and Rotor Position at Lift Off
(Rotor Traveling Toward Position Sensors)

The rotor lifts off against gravity when traveling away from the position sensors. The peak coil current of 1.4 amperes occurs 50 msec after power is turned on (Figure 3-3). After liftoff, the coil current reverses direction to keep the rotor from overshooting its equilibrium position. The integrator begins forcing the rotor to its zero current position 70 msec after liftoff. The second trace in Figure 3-3 is the signal from the position sensor illustrating rotor position during liftoff.

When the rotor is lifting off with the assistance of gravity (towards position sensors), overshoot of the coil current is a minimum (Figure 3-4) due to the smaller coil forces required.

c. Steady-State Power at 0 and 700 RPM (Suspension Electronics Only)

The measured steady-state power at zero speed was .617 watt and at 700 rpm, .673 watt. The power increase at 700 rpm is a result of a slight gain difference between the two series connected eddy-current position sensors which causes small axial rotor oscillations (150 microinches, 0 to peak) at the rotor spin frequency. The integrator time constant (.02 second) was chosen to minimize this runout at 700 rpm.

Steady-state power consists of standby power drawn from op-amps, runout power at speed, and deadband removal power. As discussed in Section 2.7, the power bridge deadband is removed by biasing the power amplifiers to the point of conduction. Power is then drawn by each amplifier from the 28 volt supply as well as that drawn from the 15 volt supply due to the biasing network. The total deadband removal power is $\approx .250$ watt.

d. Closed Loop Step Response

The output of the series connected control position sensors is shown in Figure 3-5 when the rotor is excited by a 10 Hz square wave. The rise time (from 10 to 90 percent of final amplitude) is 4 msec with the servo damping coefficient of $\delta \cong .707$. Design requirements are for the rise time to be $\leqslant 6$ msec with the damping coefficient $\delta \geqslant .6$.

VERTICAL – .5V/CM
HORIZONTAL – 20 MS/CM

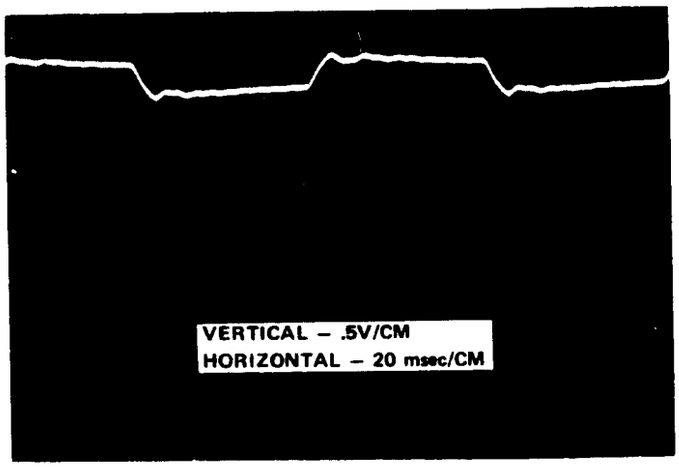

716 5-13

Figure 3-5
Axial Position Step Response (10 Hz Square Wave Excitation)

3.3 MBRW TORQUE CHARACTERISTICS

a. Spin Motor Torque

A two-phase, sine wave spin motor driver, set at 280 Hz, was used to run the redundant segmented induction motor in the MBRW. The motor terminals were connected so that the four windings that constitute each phase are in series-parallel. Motor power was measured with a phase angle voltmeter reading the voltage across a 1 ohm resistor in series with Phase A and B. The phase angle voltmeter thus measures motor winding current I cos θ. Power can then be calculated by multiplying I cos θ by the spin motor driver output voltage.

Spin motor torque was measured with a strain gauge reaction torque sensor. Figure 3-6 is a curve of motor torque versus speed with the driver voltage set for a minimum torque of .007 ft-lb (1.34 oz-in.) over ±700 rpm. The corresponding motor power for this requirement is shown in Table 3-2. The torque curves represent a net torque; motor torque less drag torque while accelerating, motor torque plus drag torque while decelerating.

Figure 3-7 is the torque curve for a minimum of .02 ft-lb (3.84 oz-in.) at any speed in any direction. Motor power for this level of torque is listed in Table 3-3. Maximum motor power is 9.6 watts to maintain the required torque over the ±700 rpm speed range.

b. Drag Torque

Initial testing revealed the rotor drag torque to be much larger than expected (.16 oz-in./1000 rpm versus .001 oz-in./1000 rpm). Preliminary investigation showed that the stray magnetic fields from the magnetic bearings were interacting with the induction motor, thereby creating rotor drag. This was proven by placing a partial magnetic shield (covering approximately 30 percent of motor) between each motor segment and the magnetic bearings. Curves 1 and 2 in Figure 3-8 show drag curves with and without shields. A 30 percent improvement resulted with the partial shield. Further tests should be conducted to explore design modifications that would reduce the drag torque in future designs. The first test would investigate the effect of reversing one of the permanent magnets in the bearings, thus changing the stray field pattern. It is expected that this will reduce the drag torque, but increase the external magnetic fields. Other modifications which shield the motor gap from the external fields are also possible. It may be noted that the shaft power at 700 rpm corresponding to the measured drag torque is only .058 watt.

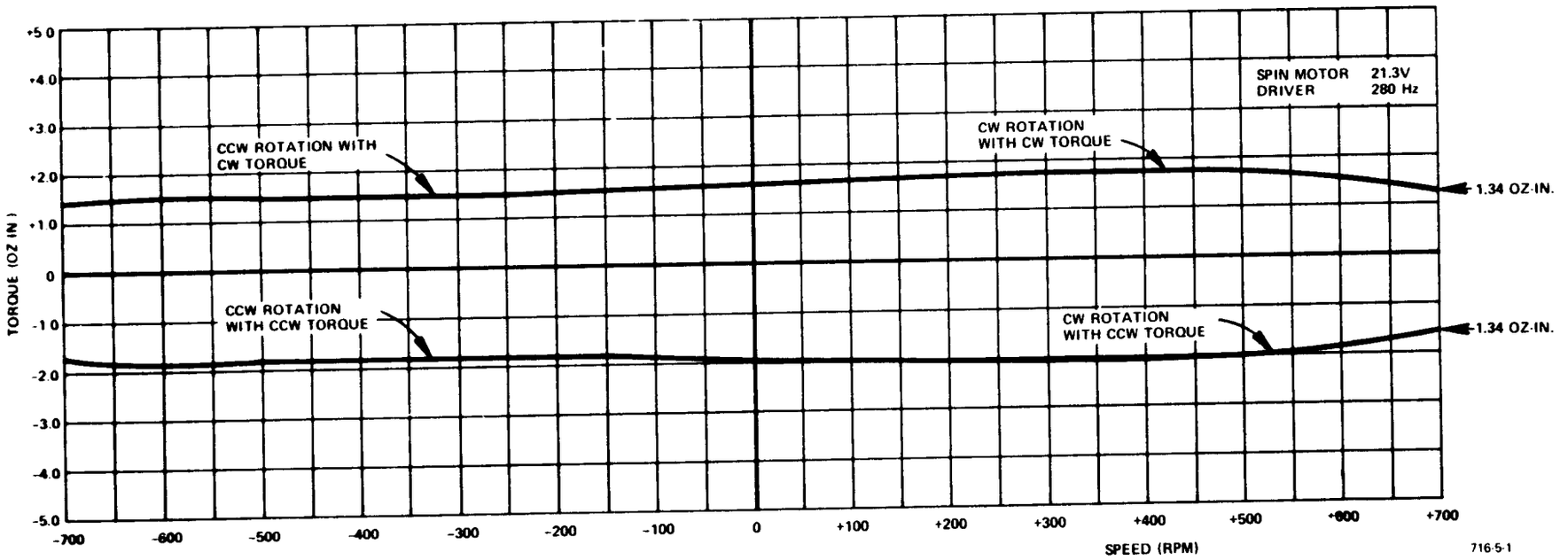

Figure 3-6
MBRW Reaction Torque, 1.34 oz-in. Minimum

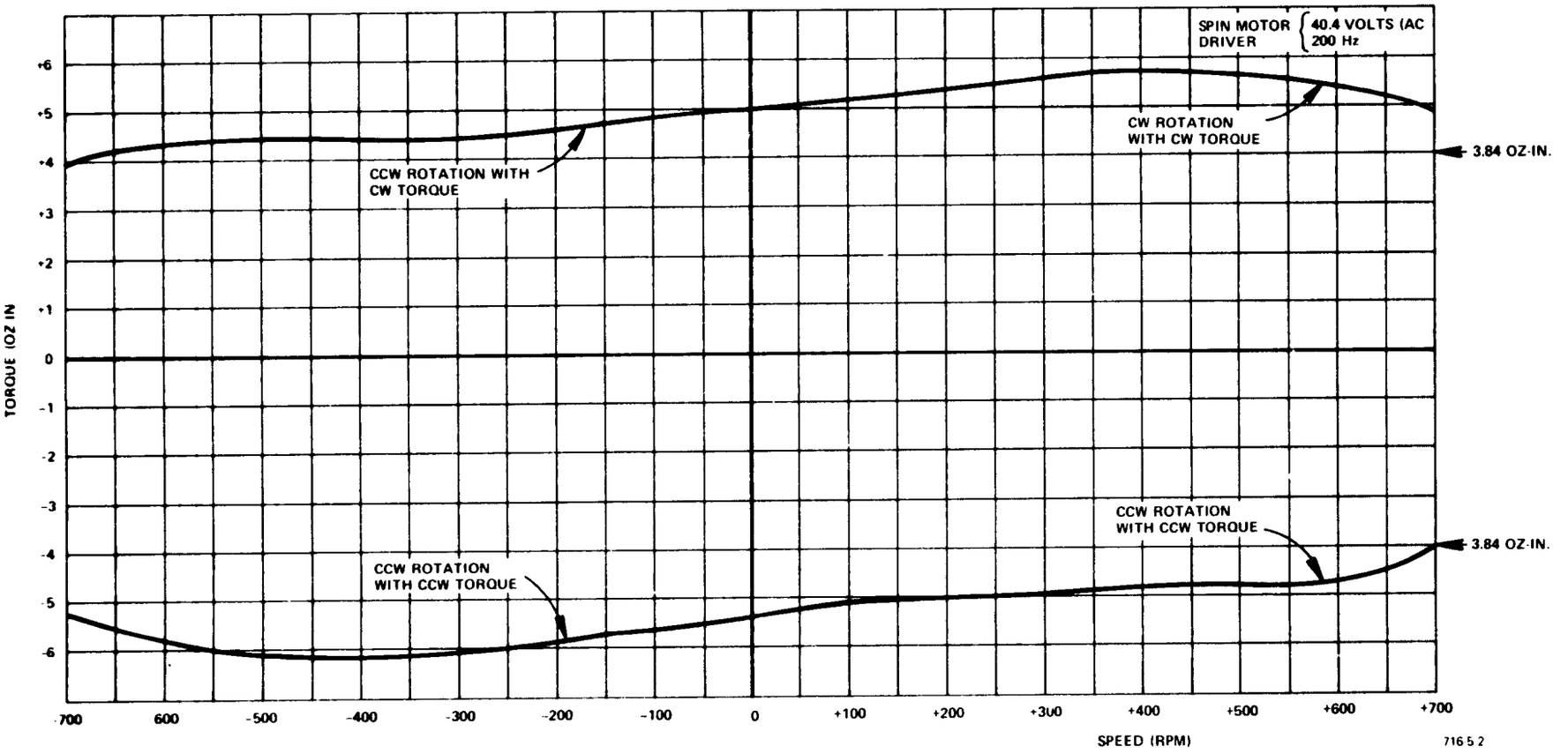

Figure 3-7
MBRW Reaction Torque, 3.84 oz-in. Minimum

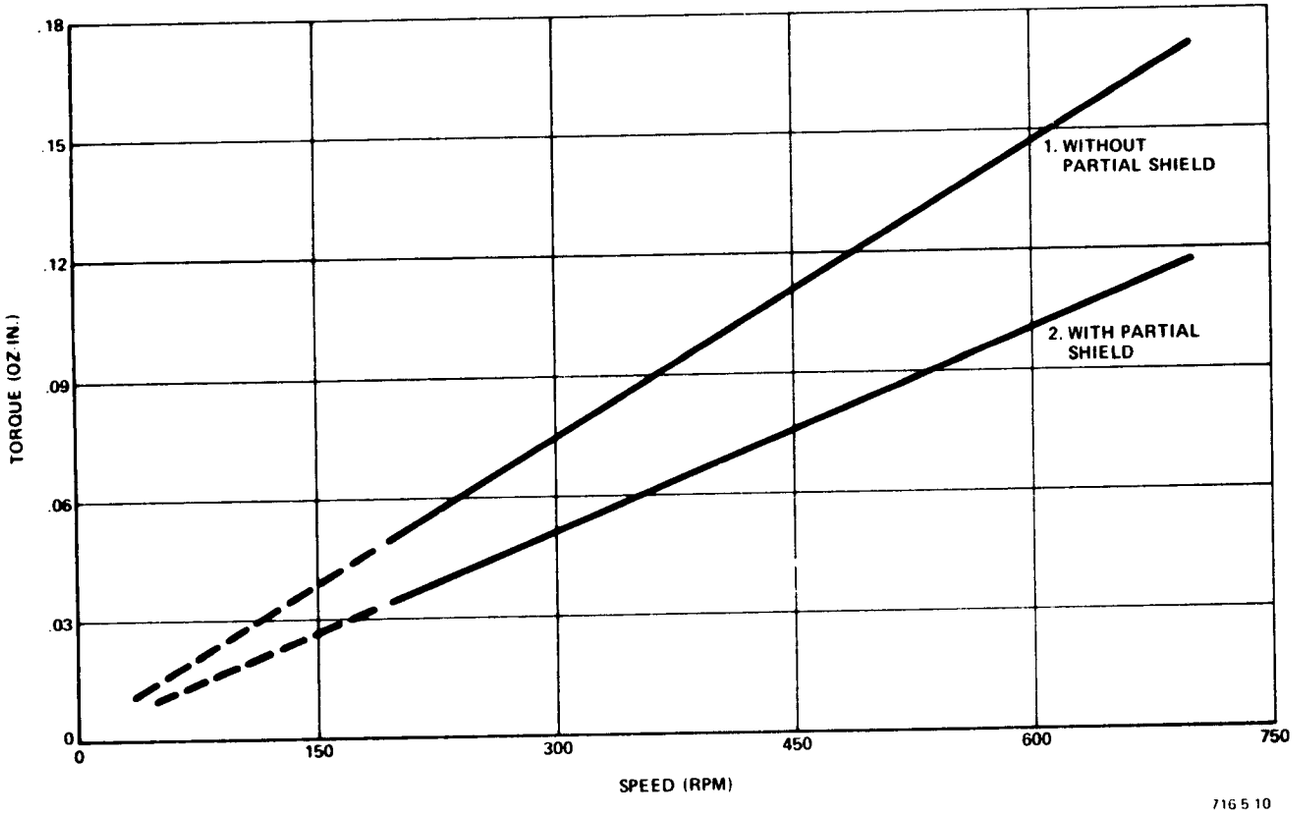

Figure 3-8
MBRW Drag Torque

TABLE 3-2

Spin Motor Driver - 21.3 vac
280 Hz
(Both Phases)

A. STALL

PHASE A			For a minimum torque of 1.34 oz-in. at any speed, in either direction.
Fwd	Icos θ = .92 amp	P = 1.96 watts	
Rev	Icos θ = .058 amp	P = 1.23 watts	
PHASE B			
Fwd	Icos θ = .072 amp	P = 1.53 watts	
Rev	Icos θ = .105 amp	P = 2.24 watts	
		Total Power	Fwd = 3.49 watts Rev = 3.47 watts

B. 400 RPM

PHASE A			
Fwd	Icos θ = .095 amp	P = 2.02 watts	
Rev	Icos θ = .053 amp	P = 1.13 watts	
PHASE B			
Fwd	Icos θ = .075 amp	P = 1.6 watts	
Rev	Icos θ = .100 amp	P = 2.13 watts	
		Total Power	Fwd = 3.62 watts Rev = 3.26 watts

C. 700 RPM

PHASE A			
Fwd	Icos θ = .085 amp	P = 1.81 watts	
Rev	Icos θ = .058 amp	P = 1.06 watts	
PHASE B			
Fwd	Icos θ = .06 amp	P = 1.28 watts	
Rev	Icos θ = .095 amp	P = 2.02 watts	
		Total Power	Fwd = 3.09 watts Rev = 3.08 watts

TABLE 3-3

Spin Motor Driver - 34.75 vac
280 Hz
(Both Phases)

A. STALL

PHASE A			For a minimum torque of 3.84 oz-in, at any speed in either direction.
Fwd	Icos θ = .155 amp	P = 5.39 watts	
Rev.	Icos θ = .09 amp	P = 3.13 watts	
PHASE B			
Fwd	Icos θ = .105 amp	P = 3.65 watts	
Rev.	Icos θ = .175 amp	P = 6.1 watts	
		Total Power	Fwd = 9.04 watts Rev = 9.23 watts

B. 400 RPM

PHASE A			
Fwd	Icos θ = .15 amp	P = 5.21 watts	
Rev	Icos θ = .105 amp	P = 3.65 watts	
PHASE B			
Fwd	Icos θ = .108 amp	P = 3.65 watts	
Rev	Icos θ = .170 amp	P = 5.91 watts	
		Total Power	Fwd = 8.86 watts Rev = 9.56 watts

C. 700 RPM

PHASE A			
Fwd	Icos θ = .152 amp	P = 5.28 watts	
Rev	Icos θ = .085 amp	P = 2.95 watts	
PHASE B			
Fwd	Icos θ = .100 amp	P = 3.47 watts	
Rev	Icos θ = .162 amp	P = 5.63 watts	
		Total Power	Fwd = 8.75 watts Rev = 8.58 watts

When operated on its touchdown ball-bearings, a relatively flat torque increase of .13 oz-in. was measured over a 300 to 700 rpm speed range.

3.4 TACHOMETER

As described in Section 2.8 the dual channel tachometer provides 520 pulses per revolution for speed determination and a direction of rotation indication. The pulses are shown in Figure 3-9 at a rotor speed of 700 rpm. This signal is the summation of the processed output of two special Bently-Nevada eddy-current probes which sense 130 teeth machined on the inside of the rotor. They are aligned such that their outputs are spaced approximately 90 electrical degrees apart.

The tachometer output pulses are 40 microseconds wide and 3.4 volts in amplitude. The uneven spacing between pulses arises from minor variations in land and groove widths. There is virtually no deadband in accurate speed output as the rotor crosses 0 rpm in changing direction of rotation. Error-free rotational direction information is also provided through 0 rpm. The power required for a single tachometer channel was .396 watt.

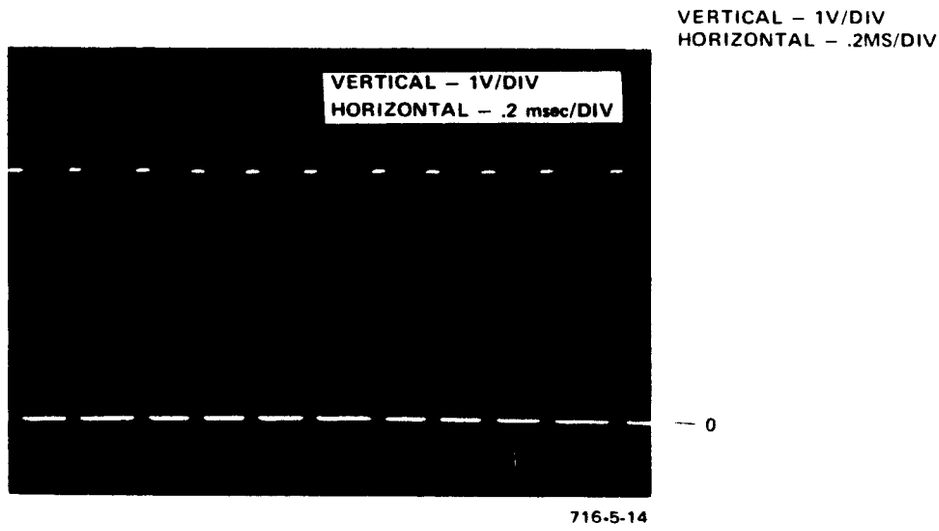

Figure 3-9
Tachometer Output Pulses (520 Pulses/Rev) at a Rotor Speed of 700 rpm

SECTION 4.0

CONCLUSIONS AND RECOMMENDATIONS

SECTION 4.0

CONCLUSIONS AND RECOMMENDATIONS

The experience gained during the construction and test of the engineering model indicates that a magnetically suspended reaction wheel is indeed applicable to interplanetary and orbiting spacecraft without appreciable penalties on weight and power. The magnetic bearing provides the capability for reliable, fully-redundant, low drag torque operation over the entire speed range, including passage through zero speed. The remainder of this section details the conclusions and outlines recommendations for further development activities.

a. Overall Performance

The concept of total redundancy of all MBRW functional systems was proven to be feasible. Thus, a weight reduction is possible when compared with a spacecraft system which utilizes a second reaction wheel to avoid single-point failures. The segmented stator construction proved the feasibility of this approach to incorporate motor redundancy. Similarly, the coils in each magnetic bearing were shown to be independently capable of controlling the axial system, so that the suspension redundancy scheme using two (redundant) position sensors and two channels of electronics is possible. The concept of using eddy-current probes to provide speed-indendent, high resolution speed sensing was demonstrated. Tachometer redundancy was proven using two identical channels (sensors and electronics).

The most significant parameters constraining the design of the magnetic bearing are the radial and angular stiffnesses. For the requirements of the specification, the angular resonance frequency constraint was the most stringent, and influenced the bearing design and hence the bearing weight. Thus, it is necessary to examine constraints on stiffness more carefully than in a conventional reaction wheel design.

Testing and evaluation of the MBRW design revealed no major shortcomings in the areas of assembly and bench operation. The design can be used directly as a basis for a flight prototype design. The overall weight may be decreased by .7 - .8 pound by the substitution of magnesium for aluminum as the material for the housings and cover. An equal weight decrease is possible if the maximum operating speed is allowed to increase to 1000 rpm; the motor power would remain within the specified requirement. A slight redesign of the configuration to eliminate the

offset of the center-of-mass from the mid-point of the bearing span would enable the achievement of 1g support with spin axis horizontal. The weight sensitivities of the design to motor power and angular momentum are: .2 lb/watt and 4.4 lb/ft-lb-sec, respectively.

The effect of structural compliance in the rotor, housing or in the mounting has the effect of introducing gain and phase peaking in the axial control loop. The web in the lower housing, for example, gave rise to a mode at 200 to 300 Hz which would necessitate complex compensation to assure axial system stability. An MBRW mount bypassing this compliance was used as the interim solution; thickening of the web to increase the structural resonance frequency is the solution for future designs. In general, the location of structural resonances below 50 Hz and above 600 Hz would be distant enough from phase crossover that single lead-lag compensation could be used. Of the two alternative spacecraft mountings, soft mounting is likely to be the more practicable approach. It is recommended that investigation of the mounting-axial system interaction be included in future development.

b. Magnetic Bearings

The angular stiffness of the bearing system was an order of 4 lower than that predicted. The relationship between geometry (bearing diameter, span) in magnetic bearing systems needs to be experimentally confirmed in order to implement suitable design modifications to increase the angular resonance frequency.

The inherent non-linearity in the control force-to-control current gain in a one-loop bearing system (if only one control coil is used) can be overcome by the use of a split-coil design, where half the winding in each bearing is at any time used for control. The failure modes in such a scheme need to be analyzed and experimentally tested to determine the effects on reliability. The use of split coils would also decrease the total current required for lift-off and hence lift-off power.

c. Motor

The weight efficiency of using the large-diameter, segmented ac induction motor concept was demonstrated. The discrepancy in drag torque appeared to be related to the interaction of the magnetic bearing stray fields with the segmented stators. The variation of motor gap fields as a function of angle around the periphery can cause additional eddy-current losses in the motor cage, leading to increased drag torque. The stray field pattern can be altered by reversing the

polarity of the permanent magnet in one bearing, with possible increase in the total external magnetic field and a decreased drag torque. Investigations aimed at drag torque reduction are recommended.

If it is desired to decrease the motor power further or to achieve a constant torque over the speed range, the possibility of using a DC brushless motor should be investigated. An ironless armature construction for such a motor would eliminate the radial unbalance otherwise characteristic of DC brushless motors.

d. Tachometer

The concept using eddy-current sensing of a periodic machined rotor profile was proven to be feasible. Further increase in tachometer resolution using this concept, however, appears difficult because of the difficulty of generating pulses of sufficient amplitude if the number of machined teeth is made any larger. A 15 percent increase in resolution would be possible if the diameter at the teeth was increased to the outside rim diameter.

e. Control System and Electronics

The use of single lead-lag compensation was demonstrated to be adequate in the absence of structural resonances in the region of phase crossover. Investigation in the following areas are recommended in order to decrease the total power consumption further:

- Use of an annular ring axial position sensor to eliminate angular mode coupling and the effect of run-out.
- Methods for decreasing the standby currents required to eliminate crossover distortion in the power amplifier.
- Possibility of using pulse width modulation in the amplifier.

SECTION 5.0

NEW TECHNOLOGY

SECTION 5.0

NEW TECHNOLOGY

The technical information contained in this report is based on prior developments at Sperry Flight Systems, in the areas of reaction wheel assemblies, motors and magnetic bearings. There was no new technology developed during the course of this contract.

APPENDIX A

ROTOR BALANCING TECHNIQUE

APPENDIX A

ROTOR BALANCING TECHNIQUE

Balancing of the MBRW rotor assembly involved some complications which are not usually encountered in balancing reaction wheel rotors:

- The rotor assembly center of gravity is offset axially from the suspension system spring and geometric centers.
- The balance correction plans are not symmetrically placed with respect to the rotor center of gravity.
- The radial proximity sensors which are used to measure rotor displacements, cannot be equally placed with respect to the rotor center of gravity or the bearing centers.

Previous balancing work with magnetically suspended rotors has involved symmetrical rotors having none of the complications listed above. This work used the fact that the low stiffness and low damping of magnetic bearings results in fairly large, easily sensed motions near critical speeds. The units were equipped with proximity sensors near each end of the shaft which gave indications of the shaft-end-motion (phase and amplitude). This sensing scheme is shown in Figure A-1. Since the proximity sensor voltage and phase information indicates total shaft-end-motions, a correction for zero-speed runout must be made to obtain the net unbalance effects. The net unbalance is then resolved into static and dynamic unbalance. This procedure is illustrated in Figure A-2.

If the rotor, suspension and balance planes are symmetric, the static and dynamic indications can be used to determine sensitivities and make balance corrections directly. In case of this MBRW, the same general procedure can be followed, but the resolution of the total unbalance into static and dynamic components requires decoupling of non-symmetric effects listed in the first paragraph. This coupling problem can be handled by relating the apparent unbalance directly to the required correction weights through influence coefficients, a_{ij}:

$$W_1 = a_{11} S' + a_{12} D' \qquad \text{(A-1)}$$

$$W_2 = a_{21} S' + a_{22} D' \qquad \text{(A-2)}$$

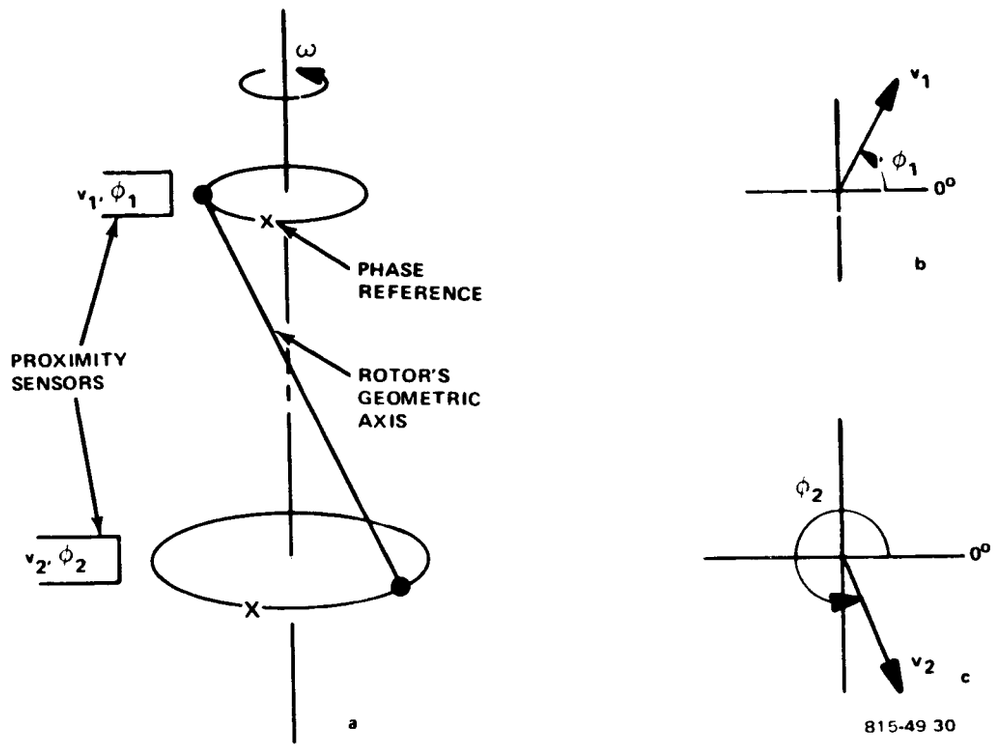

Figure A-1
Sensing Rotor Motions Due to Unbalance

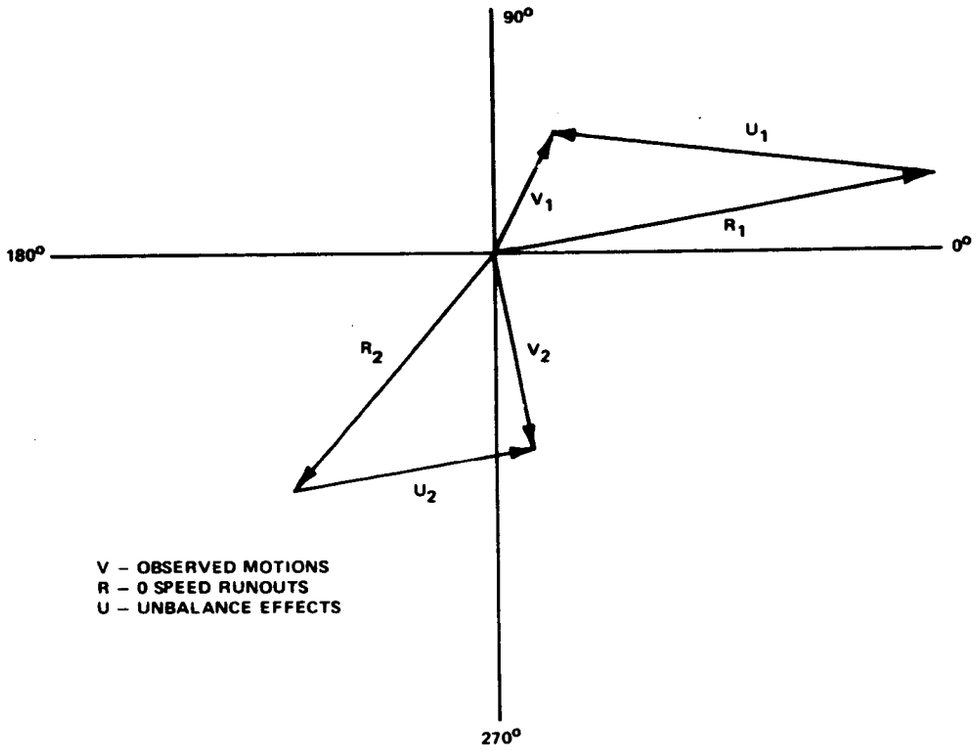

a. SEPARATION OF RUNOUT AND UNBALANCE EFFECTS

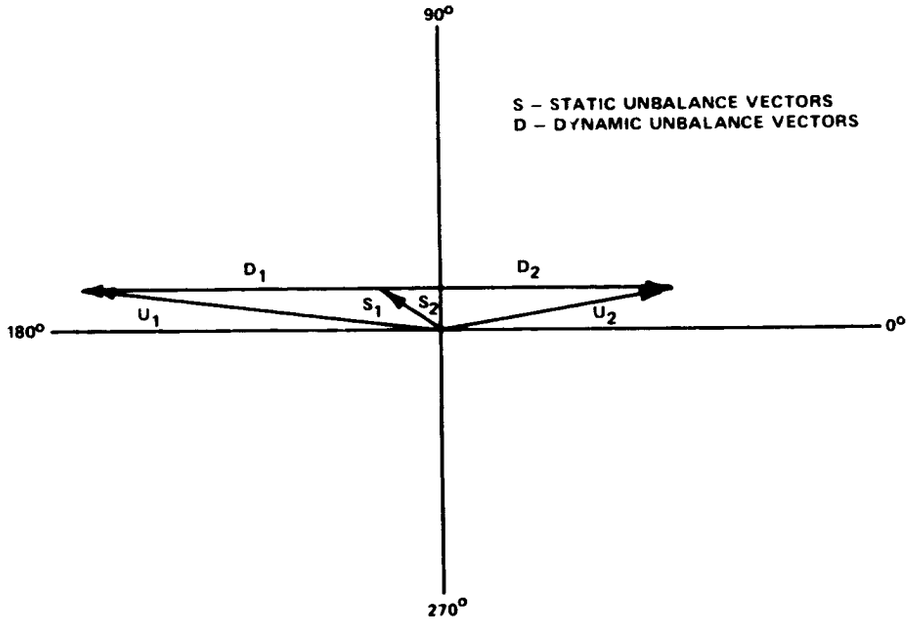

b SEPARATION OF STATIC AND DYNAMIC UNBALANCES

716-5-19

Figure A-2
Balancing Phasor Diagrams

where

W_1 and W_2 are the correction weights for plane 1 and plane 2

This relationship applies to a given phase plane in the rotor for a given speed. It can be generalized, giving,

$$\vec{W}_1 = a_{11} \vec{S}' + a_{12} \vec{D}' \tag{A-3}$$

$$\vec{W}_2 = a_{21} \vec{S}' + a_{22} \vec{D}' \tag{A-4}$$

or using matrix notation,

$$[\vec{W}] = [a] [\vec{U}'] \tag{A-5}$$

where

$$[\vec{U}'] = \begin{bmatrix} \vec{S}' \\ \vec{D}' \end{bmatrix} \tag{A-6}$$

and the a_{ij} values can be determined by trial weight additions to each of the balance planes. Since it was also required that the actual static and dynamic unbalance levels be known, another relationship is required which relates the actual unbalance to weights in the two correction planes.

$$[\vec{U}] = [b] [\vec{W}] \tag{A-7}$$

where

$$[\vec{U}] = \begin{bmatrix} \vec{S} \\ \vec{D} \end{bmatrix}$$

The b_{ij} values are determined directly from the geometry of the rotor and the placement of the correction planes.

A direct relationship can be formed between indicated and actual unbalance from equations A-5 and A-7.

$$[\vec{U}] = [B] [\vec{U}'] \tag{A-8}$$

where

$$[B] = [b] [a] \tag{A-9}$$

For the MBRW in its final configuration, the values of the coefficient matrices are:

$$[a] = \begin{bmatrix} -1.015 & 2.53 \\ 2.593 & -3.52 \end{bmatrix} \text{ at 950 rpm} \qquad \text{(A-10)}$$

$$[b] = \begin{bmatrix} .1336 & .1336 \\ .0103 & -.0835 \end{bmatrix} \qquad \text{(A-11)}$$

$$[B] = \begin{bmatrix} .211 & -.132 \\ -.227 & .320 \end{bmatrix} \text{ at 950 rpm} \qquad \text{(A-12)}$$

The 50 percent overspeed point, 950 rpm, was chosen to obtain increased sensitivity over the sensitivities at 700 rpm nominal operating speed.

Besides relating correction weights to the unbalance, the influence coefficient matrices [a] and [B] also include unit conversion factors and the calibration factors of each of the two radial proximity sensors. In the above matrices, the unbalance indications $[\vec{U}']$ are in terms of proximity sensor voltages, the weights $[\vec{W}]$ are in grams and the unbalance $[\vec{U}]$ is in oz-in. and oz-in.^{2}.

During the trial balancing, using lead tape to make corrections, it was found that using equation A-5 directly to determine correction weights, both static and dynamic unbalance levels were reduced by approximately the same factor.

The original unbalance levels in the rotor assembly were determined to be .13 oz-in^2 dynamic and .12 oz-in static. The final balance was achieved after two iterations and the residual unbalance levels are .019 oz-in^2 and .0035 oz-in.

APPENDIX B

INFLUENCE OF STRUCTURE ON THE SUSPENSION SYSTEM

APPENDIX B

INFLUENCE OF STRUCTURE ON THE SUSPENSION SYSTEM

The interaction of the suspension system with structural modes in the rotor and/or the housing can lead to complexity of the control compensation; these structural modes must therefore be designed to be outside a critical frequency band.

Examination of the axial open-loop frequency response of several magnetic suspensions at Sperry shows

(1) at several frequencies, there is a peaking of the phase characteristics where a bell-shaped characteristic is observed;

(2) at each of these frequencies, there is a gain notch followed by a gain peak.

These effects are caused by flexibilities in the housing mounting and/or in the rotor structure. The result of these structural modes is to render the task of axial stabilization of the control system more complex if the modes occur in the region of the phase crossover of the compensated characteristic. Thus, a structural mode may necessitate the use of double lead-lag compensation rather than a single lead-lag.

The analysis below incorporates a single housing flexibility in the suspension model and shows the structural interaction. The effects of flexibility in the rotor structure lead to analogous gain/phase characteristics, and a separate analysis is therefore not presented here.

This model, shown in Figure B-1, incorporates a single housing stiffness k_H and mass m_H in addition to the simple rigid body magnetic bearing model

$$m\ddot{z} - k_U z = F_{ext} + F_c.$$

The equations of motion are

$$\begin{aligned} m\ddot{z} - k_U (z - z_H) &= F_c + F_{ext} \\ m_H \ddot{z}_H + k_H z_H + k_U (z - z_H) &= -F_c \end{aligned} \qquad \text{(B-1)}$$

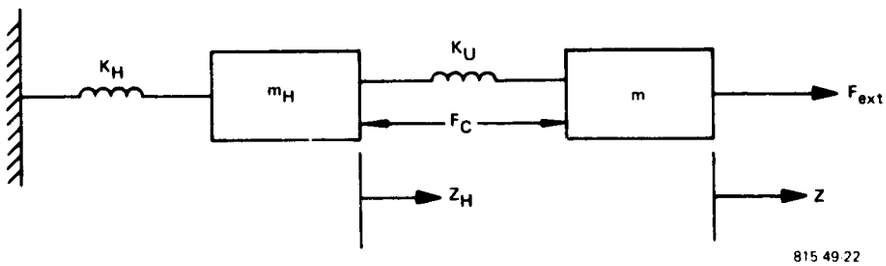

Figure B-1
Structural Model to Illustrate Effect of Housing Flexibility

where

m = the suspended mass (rotor mass)

k_U = the unbalance stiffness

F_c = the axial control force

F_{ext} = the external force

z = the inertial displacement of the rotor

and

z_H = the inertial displacement of the housing

The position sensor, mounted on the housing, senses the relative displacement $(z - z_H)$. This relative displacement is used to generate an appropriate control force F_c to overcome the axial instability. The open-loop transfer function may be determined as

$$\frac{z - z_H}{F_c} = \frac{(m_H + m)\, s^2 + k_H}{m\, m_H\, s^4 + s^2 [k_H\, m - k_U (m_H + m)] - k_H\, k_U} \qquad \text{(B-2)}$$

It can be seen that the case $k_H \to \infty$ gives back the simple model in which

$$\frac{z - z_H}{F_c} = \frac{1}{m\, s^2 - k_U}$$

The open-loop transfer function, equation (B-2), has a pair of imaginary zeros at $\pm j \left(\frac{k_H}{m_H + m}\right)^{1/2}$, a pair of imaginary poles, and two real poles, one of which is in the right-half plane (showing the static instability). Application of the Routh-Hurwitz criteria shows that the imaginary poles are always greater in magnitude than the imaginary zeros, as shown in Figure B-2. This means that the open-loop frequency response will include a phase peak (lead) and a notch-peak in the gain curve, as shown in Figure B-3.

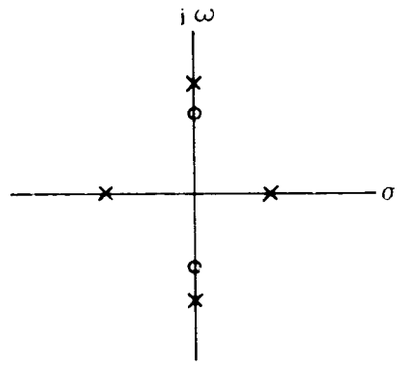

REAL POLES – SUSPENSION
IMAGINARY POLES } STRUCTURE
IMAGINARY ZEROS }

716-5-25

Figure B-2
Pole Location due to Housing Flexibility

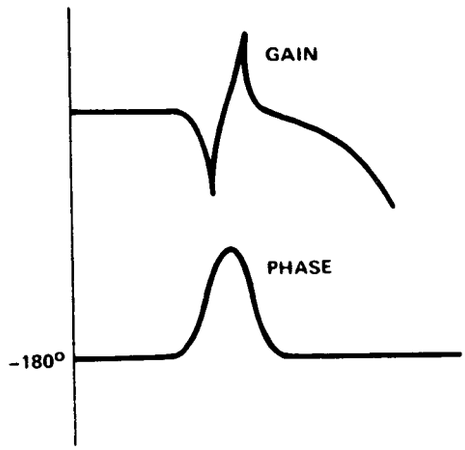

716-5-26

Figure B-3
Effect of Flexibility on Open-Loop Response

The above analysis can be extended to the real case where the lumped model includes several masses and flexibilities; the open-loop response will then exhibit the phase peak and the gain notch-peak at several frequencies, as observed in actual measured responses.

Hence, for simplicity of stabilization, it is important to design both housing and rotor structure so as to locate the structural modes either well below or well above the open-loop rigid body poles $\pm\sqrt{k_U/m}$.